frontiers in Earth Science

ORIGINAL RESEARCH
published: 07 September 2018
doi: 10.3389/feart.2018.00131

Monitoring Impacts of Urbanisation and Industrialisation on Air Quality in the Anthropocene Using Urban Pond Sediments

Ann L. Power[1], Richard K. Tennant[1], Richard T. Jones[2], Ya Tang[3], Jie Du[3], Annie T. Worsley[4] and John Love[1]*

[1] Biosciences, BioEconomy Centre, University of Exeter, Exeter, United Kingdom, [2] Geography, University of Exeter, Exeter, United Kingdom, [3] College of Architecture and Environment, Sichuan University, Chengdu, China, [4] Strata Environmental, Wester Ross, United Kingdom

OPEN ACCESS

Edited by:
Graeme Thomas Swindles, University of Leeds, United Kingdom

Reviewed by:
Mingrui Qiang, Lanzhou University, China
Nadia Solovieva, University College London, United Kingdom

***Correspondence:**
Ann L. Power
a.power@exeter.ac.uk

Specialty section:
This article was submitted to Quaternary Science, Geomorphology and Paleoenvironment, a section of the journal Frontiers in Earth Science

Received: *14 May 2018*
Accepted: *13 August 2018*
Published: *07 September 2018*

Citation:
Power AL, Tennant RK, Jones RT, Tang Y, Du J, Worsley AT and Love J (2018) Monitoring Impacts of Urbanisation and Industrialisation on Air Quality in the Anthropocene Using Urban Pond Sediments. Front. Earth Sci. 6:131. doi: 10.3389/feart.2018.00131

The release of toxic atmospheric pollutants since the Industrial Revolution is a major global challenge, driving climate change and damaging human health. Spatial health inequalities highlight the need to explore air pollution in different localities throughout the Anthropocene. Air quality monitoring programmes are spatially and temporally limited. We show how suitable urban sediment archives provide site specific records of long-term particulate matter (PM) releases, in cities and urban landscapes, that are or have been subjected to high pollution levels. High-resolution PM records spanning from the mid-20th century were reconstructed from an urban pond in Chongqing, southwest China, one of the fastest growing Chinese urban centres in the late 20th century. Temporal variations in pollution proxies including geomagnetic, geochemical and spheroidal carbonaceous particle trends correspond to key phases of industrial and urban developments, that are representative of the locality. Observed increases in air pollution proxies post-1960 coincide with the location of military-related industries to Chongqing and industrial intensification. Post-1997 pollution mirrors rapid urbanisation that occurred following the designation of Chongqing as a government-controlled municipality at this time and reveals a steadily increasing pollution trend to present day (2015). In comparison to Chongqing, an atmospheric depositional history was constructed from an urban pond in the Merseyside region of northwest England that has experienced a legacy of contamination since the early 19th century. In northwest England, changing characteristics of pollution are related to the establishment of localised, modern industries, power generation, urban sprawl, increased combustion-derived pollution post-1990 and effective pollution legislations. Whereas a reduction in air pollution has occurred post-2000 in Merseyside, in Chongqing, however, air pollution has continued to increase in spite of national efforts in pollution control. These urban sediments reveal the changing nature of air pollution in different urban landscapes, allowing us to assess air quality impacts of progressive industrial activity, increased road and air travel, urban expansion and the efficacy of

pollution controls. It appears that air pollution remains an inevitable consequence of global industrialisation. It is therefore crucial to understand pollution histories in densely populated urban regions to determine environmental burdens of pollution on health over generational timescales.

Keywords: air pollution histories, urban ponds, geochemistry, geomagnetism, SCP, urbanisation

INTRODUCTION

Air pollution is a crucial challenge of the Anthropocene threatening the stability of Earth systems, driving global climate change, destroying ecosystems and endangering human health (Rockström et al., 2009). Exposure to air pollution is now recognised as responsible for 16% of all global deaths with poor and vulnerable populations disproportionately affected and children at high risk of illness from exposure to even very low levels of toxic air (Landrigan et al., 2017).

A range of environmental toxins has been released into the atmosphere due to urbanisation and industrialisation over the last 200 years (Brimblecombe, 2005; Thevenon et al., 2011; Chen et al., 2016). Industrialised urban development has occurred at varying times across the globe. Since the onset of the Great Acceleration (post-1950) extensive pollutant emissions have dramatically altered the composition of the atmosphere and degraded air quality at global, regional and local scales (Rose et al., 2004) with severe levels of air pollution regularly experienced in a number of different cities (Han et al., 2015). However, as air quality data are both spatially and temporally limited the consequential health effects of long-term (>20 years) exposure to air pollution for urban populations are unknown (Taubes, 1995).

In the United Kingdom, the legacy of industrial urbanisation dates from the Industrial Revolution (post-1800) during which time Britain experienced a period of 'Great Acceleration.' Since then, pollution releases reflect industrial intensification, shifts in technologies, fuel consumption trends and power generation, transport activities and the introduction of pollution controls. The chronic effects of fossil fuel emissions on air quality and public health were unequivocally realised in Britain after the infamous London Smog in 1952. The estimated deaths of approximately 3,000 – 4,000 people following the Smog (Bell et al., 2003) resulted in air quality legislation (Clean Air Act, 1956), which overtime became increasingly stringent. The Smog also instigated nation-wide air quality monitoring such as the National Survey (post-1961) and the Automated Urban and Rural Network since 1998. Despite the known environmental and public health risks, it seems as though global environmental degradation is an inevitable accepted consequence of economic growth and urban development with attempts at pollution control a secondary consideration following the recognition of wide-scale health impacts or environmental destruction (Kahuthu, 2006).

Whereas Britain experienced a more progressive history of urban development lasting 200 years, in China, rapid urban transformation has occurred during the past few decades (OCED, 2018). Extensive economic growth and industrial intensification since the establishment of the People's Republic of China in 1949 has resulted in extreme environmental degradation (Zhang et al., 2014). Air quality deterioration in China is demonstrated by regularly occurring urban smog and some of the highest ever recorded pollution levels (World Health Organisation, 2014b; Kulmala, 2015).

Atmospheric particulate matter (PM_{10} and $PM_{2.5}$) are a major environmental concern. Released from natural, industrial, transport and domestic sources, fine PM are burdened with toxic heavy metals and are small enough to penetrate deep into the lungs (Chen and Lippmann, 2009). $PM_{2.5}$ are responsible for an estimated 3 million annual deaths worldwide (Silva et al., 2013; World Health Organisation, 2014a). Health effects of PM_{10} and $PM_{2.5}$ exposure include pulmonary disease, heart disease, stroke, asthma, cancers and premature mortality (Pope and Dockery, 2006; Anenberg et al., 2010; Pope et al., 2011; Beelen et al., 2014; Brugha and Grigg, 2014; Brugha et al., 2014). Human exposure to PM depends, in part, on locality with higher ambient PM concentrations experienced within industrial landscapes and cities where people, traffic, industries and, therefore, pollutants are concentrated.

Annual average concentrations of PM_{10} in 31 principle capitals of China are reported to have reduced from 120 $\mu g\ m^3$ in 2001 to 100 $\mu g\ m^3$ in 2008 (Kan et al., 2012); however, this ambient concentration vastly exceeds the WHO standard of 40 $\mu g\ m^3$. The economic cost of health burdens relating to PM_{10} exposure in China's largest 111 cities was CNY 184,761 million (GBP 21,483 million) in 2004 (Zhang et al., 2008). Clusters of disease and a rise in 'cancer villages' across China have been identified (Liu, 2010). Lung cancer rates in China have increased by 465% since 1980. Lung cancer is the leading cause of cancer in urban areas (Zhao et al., 2010) and significant effects of outdoor air pollution on mortality from lung cancer have been observed (Cao et al., 2011).

Located in the upper Yangtze River basin in southwest China, Chongqing is the most populated municipality in China. Home to 30.17 million inhabitants, Chongqing experiences among the highest levels of air pollution in the world (Yongguan et al., 2001; Kan et al., 2012). The mountainous topography and subtropical, humid, monsoon climate of Chongqing prevents the dispersal of airborne pollutants (Chen and Xie, 2013). Annual urban mean $PM_{2.5}$ concentrations were 75.4 ($\pm$42.2) $\mu g\ m^3$ in 2012–2013 (Chen et al., 2017). However, in 1995 a daily mean $PM_{2.5}$ concentration of 147 $\mu g\ m^3$ was measured in Chongqing, reaching a maximum of 666 $\mu g\ m^3$ (Venners et al., 2003).

Fuel combustion, industry, mining, the application of agricultural pesticides and fertilisers, trains, shipping, road and air travel all contribute to PM_{10} and $PM_{2.5}$ emissions. China is the largest global consumer of coal (BP, 2017). Whereas national

coal consumption has declined since 1956 in the United Kingdom (Carbon Brief, 2015), China still commissions new coal fired power stations (Chang et al., 2016). However, the aforementioned recent reductions in PM_{10} and $PM_{2.5}$ potentially reflect the establishment of ambient air quality standards in China since 2012, that set daily and annual average limits of $PM_{2.5}$ and PM_{10}, and reports hourly pollution concentrations monitored at 945 sites in 190 cities (Rohde and Muller, 2015).

Despite recent national air quality monitoring schemes in China and the United Kingdom, available data are spatially and temporally limited. Furthermore, the composition and source of PM are not determined. We therefore utilised urban sediment archives to reconstruct long-term (>50 years) histories of air pollution from a heavily industrialised urban landscape of Chongqing, southwest China. Geomagnetic, geochemical, spheroidal carbonaceous particle (SCP) and radiometric analyses were applied to the sediments of Sky Pond (SKP) to assess the anthropogenic deposition of pollutants throughout the 20th century. The global and temporal significance of Chongqing's air pollution record is contextualised *via* comparison with an air pollution history reconstructed from an urban pond [Dogs Kennel Clump (DKC)] set in the industrial birthplace of the United Kingdom: Merseyside in northwest England.

Extending our knowledge of how air pollution characteristics have changed throughout the Anthropocene, in localities with differing patterns of industrial and urban development is crucial for understanding site-specific pollutant releases and to assess the effectiveness of air quality legislations. Most importantly, understanding the types of pollutants urban residents are exposed to over their own lifetimes is crucial for identifying the long-term health burdens for both local and global populations, and to help protect human health in the future.

MATERIALS AND METHODS

Sky Pond Site Description and Urban Setting

Sky Pond (SKP) is located in Chabao, a village in Jiulongpo District, central Chongqing, in southwest China (29°26′53.37″N, 106°23′9.69″E) (**Figure 1**). Chongqing, a highly urbanised megacity, is currently experiencing rapid urbanisation and industrialisation. SKP is situated at an altitude of 506 m above ordnance datum (AOD) within the Zhongliang Mountains, elevated above the industrial district of Daduko < 4.7 km east (at ∼200 m AOD), and the industrialised Yangtze River ∼10.6 km east (at ∼200 m AOD). The local geology is comprised of Upper Permian, Lower and Middle Triassic limestones, calcareous mudstones, gypsum, marls and dolomites (Chen et al., 2016).

Situated within a mountain basin, SKP is a closed system with no inflows or outflows. The pond potentially receives runoff from woodland hills, east of the pond, that incline to ∼580 m AOD (at 0.6 km to the east), however, the catchment of the pond is constrained by a stone wall that surrounds the majority of the pond circumference, and concrete steps on the western margins. The land surrounding the pond to the north, west and south is less elevated inclining to 527 m AOD (0.25 km to the west). Therefore, catchment-derived material is expected to be negligible.

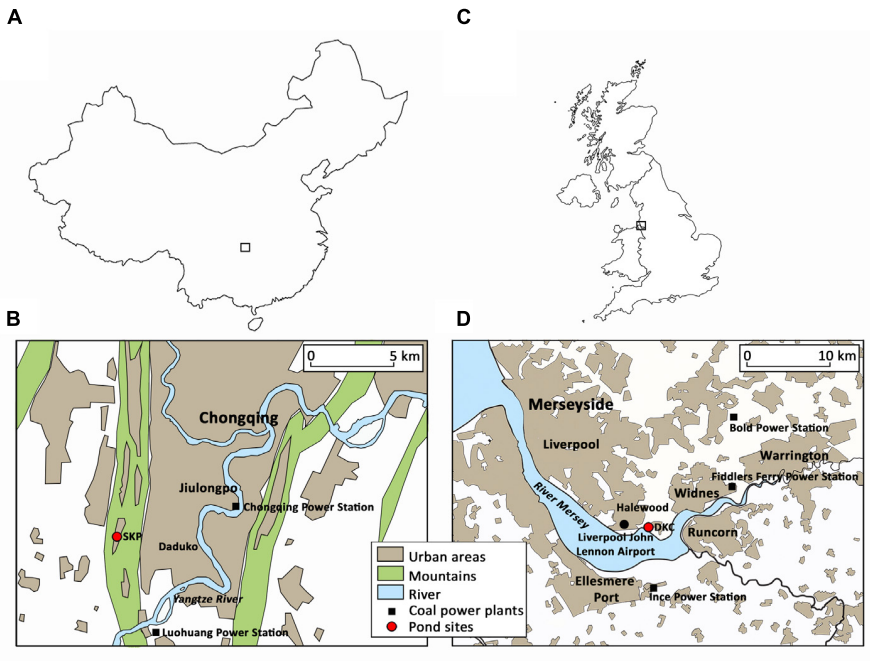

FIGURE 1 | Location of Sky Pond (SKP) in Chongqing **(B)**, southwest China **(A)** and Dogs Kennel Clump Pond (DKC) in the Merseyside region **(D)**, northwest England, United Kingdom **(C)**.

At the time of collection, SKP measured approximately 23,727 m^2, with a maximum water depth of 1.4 m, however, since then the pond has reduced to <1,100 m^2, potentially due to increased urbanisation in the area, which includes the construction of a major multilane road tunnel through the Zhongliang Mountains. Local knowledge gained from residents of Chabao, dates the existence of the pond to at least 100 years, and revealed that the pond had 'dried up' during 1961. The pond and its catchment are expected to have experienced minimal change and disturbance until very recent (post-2010) localised urban development, with the construction of an adjacent residential village, and nearby cement works (750 m south) and surrounding industries. Located adjacent to the megacity of Chongqing, the region has experienced extensive urban and industrial expansion and intensification during the 20th century.

Dogs Kennel Clump Pond Site Description and Urban Setting

Dogs Kennel Clump Pond (DKC) (53°19′59.03″N, 2°48′25.83″W) is located within the village of Hale situated in the heavily industrialised urban landscape of the Merseyside region, northwest England (**Figure 1**). DKC is <13 km southeast of the City of Liverpool and within close proximity of the heavily industrialised towns of Widnes (∼5 km east), Runcorn (<4 km southwest), Ellesmere Port (<8 km southwest) and Warrington (<9 km northeast). The region is dominated by chemical industries, oil refineries and power stations located along the coast of the River Mersey, a heartland of the Industrial Revolution since the early 1800s. Less than 3 km northwest of Hale is an industrial estate which includes chemical and pharmaceutical manufacturing and a motor car production works. DKC lies directly beneath the landing pathway of Liverpool John Lennon International Airport (<3 km west).

Dogs Kennel Clump is a small (1650 m^2, 3 m maximum water depth) human-made, agricultural pond located at 15 m AOD. It is a closed system, with no drainage outflows and a negligible catchment defined by steep, vegetated pond margins. The surrounding geology comprises Shirdley Hill Sand Formation deposits overlying Chester Pebble Beds Formation bedrock. Originally a marl pit, the pond has experienced minimal change in size and shape, revealed by historic maps [Cheshire County Series 1:10560 first edition (1881) and second revision (1911)] which traced the existence of the pond to pre-1900. Hale has remained a small village since the mid-19th century, around which the conurbations of Liverpool and Widnes have grown. The broader surrounding region has experienced major urban expansion since the Industrial Revolution and throughout the 20th century.

Sediment Core Retrieval

A Uwitech gravity corer was deployed from a small inflatable boat to collect sediment cores from the centre of the pond basins. At SKP two sediment cores (SKP1 and SKP2) were extracted on 15/09/2015. The cores were immediately extruded into 0.5 cm intervals after collection and transported back to the United Kingdom. At DKC, cores were extracted on 19/09/2013, to supplement sediment cores originally collected in 2001, to obtain the most recent history of sediment deposition. Cores were stored at 5°C, extruded into 0.5 cm intervals and freeze dried. For SKP, core SKP1 is presented as the master core, supported by evidence for SKP2, and for DKC, results are presented from DKC2 (collected in 2013) with supporting evidence from DKC1 (collected in 2001).

Geomagnetism

The geomagnetic properties of SKP and DKC sediments were determined by magnetic susceptibility, anhysteretic remanent magnetisation (ARM), and isothermal remanent magnetisations (IRM) (Walden et al., 1999). A Bartington MS2B sensor and MS2 metre was used to measure low (0.46 kHz) and high (4.6 kHz) frequency magnetic susceptibility (Walden et al., 1999). Ferrimagnetic concentration was determined by low frequency susceptibility normalised for sample weight (χ_{LF}). Susceptibility frequency dependence (χ_{FD}) was calculated as the percentage difference between high and low magnetic susceptibility frequencies to determine the contribution of superparamagnetic grains (<0.05 μm).

A Molspin AF demagnetiser was used to impart an ARM in samples whereby a peak alternating field of 100 mT was induced with a DC biasing field of 0.04 mT. Remanence was measured in a Molspin magnetometer. Results were normalised for the biasing field and are termed susceptibility of ARM (χ_{ARM}). ARM and χ_{ARM} are sensitive to concentrations of fine-grained (stable single domain, SSD) magnetic particles (Oldfield, 2007).

SIRM and backfield IRMs were induced in samples using a Molspin Pulse Magnetiser with programmed magnetic field intensities of 800 mT (SIRM) and backfield IRMs of 20 mT ($SOFT_{20}$), 100 and 300 mT ($HARD_{300}$). Remanence magnetisations were measured by a Molspin magnetometer. SIRM reflects the concentration of all remanence-carrying minerals, whereas $SOFT_{20}$ and $HARD_{300}$ show the relative amount of ferrimagnetic (e.g., magnetite) and antiferromagnetic (e.g., haematite) minerals, respectively.

SIRM and $SOFT_{20}$ are routinely used as proxies for pollution particulates due to the production of magnetite spherules from the combustion of fossil fuel (Hunt, 1986; Matzka and Maher, 1999; Yang et al., 2009; Oldfield, 2014). $HARD_{300}$ has also shown to be an effective tracer of fly ash due to the haematite component of inorganic ash spheres released from fuel combustion (Hunt, 1986; Oldfield, 2014).

S-RATIO was calculated as the ratio of 100 mT to SIRM and is indicative of mineralogy. Values < -0.7 demonstrate coarse ferrimagnetic grains; -0.4 to -0.6 highlight a dominant SD ferrimagnetic component with a mix of antiferromagnetic grains; and > -0.3 suggest a dominating antiferromagnetic component (Robinson, 1986; Dekkers, 1997).

Inter-parametric ratios SIRM/ARM and SIRM/χ_{LF} highlight changes in magnetic grains sizes if the magnetic mineralogy is uniform down-core. SIRM/χ_{LF} values can also be used to identify dominating magnetic mineralogy (Thompson, 1980; Maher and Thompson, 1999).

Geochemistry

Geochemical analysis was performed on samples at 1 cm intervals. Sediments were digested in HNO_3 and HCl (37%), filtered through Whatman 42 filters, and made up to 25 ml volumes. Geochemical analysis was performed using inductively coupled plasma optical emission spectroscopy (ICP-OES) using a Varian VISTA-MPX CCD Simultaneous ICP. Results were calibrated using a range of dilution strengths of standard solutions (1000 mg/l) of CertiPUR mix containing Ag, Al, B, Ba, Bi, Ca, Cd, Co, Cr, Cu, Fe, In, K, Li, Mg, Na, Mn, Pb, Tl, and Zn. Duplicate samples and quality control samples (concentrated at 4 ppm) were also measured to ensure precision. Element concentrations below the detection limits are excluded.

Organic Matter Content

Loss on ignition (LOI) was used to determine the organic content of sediment samples. Igniting samples at high temperatures oxidises organic carbon to carbon dioxide and ash; therefore, organic matter is approximated by post-ignition weight loss (Heiri et al., 2001). Samples were heated overnight at 105°C to initially determine moisture content, prior to exposure at 550°C for 4 h.

Radiometric Dating

Radiometric isotope chronologies were determined at the Liverpool University Environmental Radioactive Laboratory. ^{210}Pb, ^{226}Ra, and ^{137}Cs isotopes were measured *via* direct gamma assay, using Ortec HPGe GWL well-type coaxial low background intrinsic geranium detectors (Appleby and Oldfield, 1978). ^{210}Pb was determined *via* its gamma emissions at 46.5 keV, and ^{226}Ra by the 295 keV and 352 keV γ-rays emitted by its daughter isotope ^{214}Pb following 3 weeks storage in sealed containers to allow radioactive equilibration. ^{137}Cs was measured by its emissions at 662 keV. The absolute efficiencies of the detectors were determined using calibrated sources and sediment samples of known activity. Corrections were made for the effect of self-absorption of low energy γ-rays within the sample (Appleby, 1992).

^{210}Pb Dates were corroborated using the ^{137}Cs concentration peak, that reflects the 1963 fallout maximum from the atmospheric testing of nuclear weapons (Appleby et al., 1986). Sedimentation accumulation rates (g cm^{-2} y^{-1}) derived from the ^{210}Pb chronology were used to convert down-core geomagnetic, geochemical and SCP concentrations into flux profiles, to normalise for changing sedimentation rates over time (g cm^{-2} y^{-1}) (Norton et al., 1992).

Spheroidal Carbonaceous Particle Analysis

Spheroidal carbonaceous particles were used as unambiguous tracers of fossil fuel combustion, distinguished by their near-spherical, black appearance (Rose, 2015). SCPs were extracted from sediments at 2 cm intervals by sequential incubations in HNO_3, HF, and HCl (Rose, 1994). Samples were spiked with a known concentration of *Lycopodium* pollen to calculate particle concentrations. *Lycopodium* pollen grains and SCPs were identified under a light microscope (400× magnification) according to criteria for SCP identification (Rose, 2008) and quantified.

Statistical Analyses

All statistical analyses were performed using JMP Pro (Klimberg and McCullough, 2016). Pearson product moment correlation coefficients, and *p*-values were determined to assess linear relationships between down-core concentrations of elements, magnetic grains and SCPs (Singh et al., 2005). Principle component analysis (PCA) was performed on the correlation coefficient matrix to determine the dimensionality of the data set, allowing characterisation from a reduced set of factors (Kim and Kim, 2012). Principle components (PC) with eigenvalues >1 were used to assess the variance of data. Cluster coefficients from the PCA were used to support the determination of groups of variables exhibiting significant mutual correlations.

RESULTS

Results from SKP, the focus of this paper, are presented in detail in the following section. All results and interpretations for the geomagnetic, geochemical, SCP and radiometric analyses of DKC sediments, presented as a comparative study in this work, are provided in the **Supplementary Information** and are referred to in the discussion (section "Comparison of Air Pollution Histories From Chongqing and Merseyside").

Stratigraphy Integrity and Sediment Chronology

An unequivocal, intact, high-resolution (52 years in 26 cm) sediment chronology was achieved for SKP1 using radiometric dating (**Figure 2** and **Tables 1**, **2**). The pre-1960 basal layer, below 28 cm, is characterised by compact sediment, exhibiting low χ_{LF} (<0.25 10^{-6} m^3 kg^{-1}) reflecting the diamagnetic effect of relatively higher organic matter content (10–15%) (**Supplementary Figure S1**). Increased bulk density below 28 cm reflects a drying episode within the catchment during 1961, informed (to us) by local residents and confirmed by an episode of slow sediment accumulation at this depth. Due to uncertainty in the pre-1961 sediments (below 28 cm), we focused on the sediment record above this depth, which exhibits an overall decline in sediment compaction to the top of the core and relatively constant organic inputs (<10%).

^{210}Pb dates, calculated using the constant rate of supply model (Appleby and Oldfield, 1978), assign 1963 at a depth of 23–24 cm. This is corroborated by peak concentrations of the artificial isotope ^{137}Cs at 26.5 cm, a marker for the maximum atmospheric fall out from nuclear weapons testing during this year (**Figures 2**, **3**). Due to the high-resolution nature of the sediment chronology, this discrepancy is small. Sedimentation rates steadily increase to the surface of the core, from a mean value of 0.16 g cm^2 y^{-1} (0.30 cm y^{-1}) during the 1960s and 1970s to 0.42 g cm^2 y^{-1} (1.3 cm y^{-1}) post-2010. These steadily increasing sedimentation trends suggest that sporadic sedimentation events from potential catchment-disturbances have been minimal.

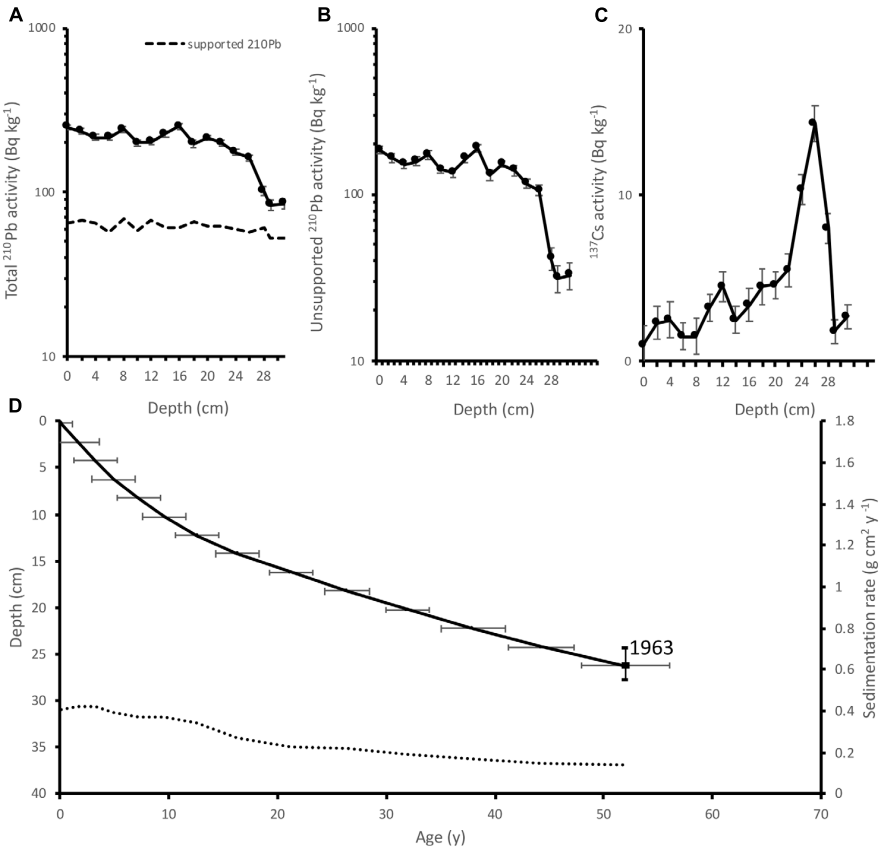

FIGURE 2 | Sediment chronology for Sky Pond (SKP 1) determined by radiometric dating (**Table 1**), showing down-core activities for **(A)**: total and supported ^{210}Pb, **(B)** unsupported ^{210}Pb as calculated by subtracting ^{226}Ra activity from total ^{210}Pb activity, and **(C)** ^{137}Cs activity. **(D)** Sedimentation rates (dotted line) and ^{210}Pb dates (**Table 2**) were derived from the constant rate of supply (CRS) model and corrected using the ^{137}Cs peak resulting from nuclear weapons testing in 1963. Since total ^{210}Pb activity **(A)** is still significantly above that of the supporting ^{226}Ra in the deepest sample analysed, at 31–31.5 cm, it appears that the core spans a period of no more than a few decades. ^{137}Cs activity in the core has a well resolved peak at 26.25 ± 1.75 cm that records the 1963 fallout maximum from the atmospheric testing of nuclear weapons **(C)**. Corrected ^{210}Pb dates have been calculated using the 1963 ^{137}Cs date as a reference point. The results are unequivocal for the post-1963 period. During that time sedimentation rates increased from a mean value of 0.16 g cm^{-2} y^{-1} (0.30 cm y^{-1}) during the 1960s and 1970s to 0.42 g cm^{-2} y^{-1} (1.3 cm y^{-1}) during the early 21st century.

Stratigraphic comparisons of magnetic concentrations (χ_{LF}) between two cores collected from SKP (SK1 and SKP2) show excellent agreement (**Supplementary Figure S1**). Intra-basin reproducibility indicated by with well-matched magnetic horizons at corresponding core depths confirms that sediments have not been disturbed by dredging or de-silting practises and that sedimentation has occurred uniformly within the basin. Furthermore, periodical drying of the pond is excluded by the lack of 'noisy' χ_{LF} profiles, allowing confidence in the integrity of the sediment record.

Geomagnetic, Geochemical and SCP Concentrations

Down-core geomagnetic, geochemical and SCP concentrations recorded in SKP sediments are presented (**Figure 3**). The basal sediments (below 28 cm), for which the depositional history is uncertain, demonstrate low magnetic concentrations (χ_{LF}, SIRM and $SOFT_{20}$) characterised by relatively fine magnetic grains (high χ_{ARM}, and low SIRM/ARM) and relatively high Al, Cu, K, and Ni. There is a distinct shift in the magnetic record above this layer with elevated χ_{LF}, SIRM, $SOFT_{20}$, Cd, Ca, Cu, Pb, Mn, Tl, Zn, and SCPs. Post-1997 (0–14.5 cm) high concentrations of Zn, Tl, Mn, Pb, and Cd are sustained, Al, Ca, Cu, K, and Ni concentrations are reduced, and SIRM, $SOFT_{20}$, χ_{LF}, and χ_{ARM} steadily decline to the surface. Consistent SIRM/ARM values suggest minimal variation in the size of magnetic grains throughout the core. $HARD_{300}$ is relatively constant and $SOFT_{20}$ concentrations exhibit an overall decline with peaks at 8 and 25 cm. SCPs exhibit relatively low values at the start of the atmospheric record: 16140 g^{-1} (number of SCPs per mass of sediment) at ∼1961 (27 cm), with maximum concentrations: 121,886 no. g^{-1} at 1980 (21 cm), and a second peak of 88,290 g^{-1} in recent sediments (2 cm, corresponding to 2013).

Magnetic grains can derive from direct atmospheric deposition (e.g., pollution particles), the surrounding catchment (e.g., soil grains) or *in situ* formation (e.g., bacterial magnetosomes, reduction diagenesis and post depositional

TABLE 1 | Fallout radionuclide concentrations in Sky Pond SKP corresponding to **Figure 2**.

		^{210}Pb						^{137}Cs	
Depth		Total		Unsupported		Supported			
cm	g cm^{-2}	Bq kg^{-1}	±	Bqkg^{-}	±	Bqkg^{-1}	±	Bqkg^{-1}	±
0.25	0.06	248.5	9.4	184.3	9.6	64.2	2.0	1.0	1.1
2.25	0.67	234.6	9.7	166.8	10.0	67.8	2.2	2.3	1.0
4.25	1.33	216.1	8.3	151.5	8.5	64.7	1.9	2.5	1.1
6.25	2.07	215.3	9.7	158.2	9.9	57.1	1.9	1.5	0.8
8.25	2.89	240.7	10.2	172.5	10.5	68.3	2.4	1.5	1.1
10.25	3.78	199.4	6.5	140.5	6.6	58.9	1.5	3.2	0.8
12.25	4.89	202.5	7.7	134.5	7.8	67.9	1.8	4.5	0.9
14.25	6.07	226.2	8.4	164.9	8.5	61.2	1.7	2.5	0.8
16.25	7.20	251.6	8.8	190.2	9.0	61.4	1.7	3.4	1.0
18.25	8.34	197.5	9.1	131.4	9.3	66.1	2.0	4.5	1.1
20.25	9.50	213.2	7.0	151.6	7.2	61.5	1.5	4.6	0.8
22.25	10.54	200.6	8.9	138.7	9.1	61.9	1.9	5.5	1.0
24.25	11.55	175.3	6.7	115.6	6.9	59.8	1.5	10.3	0.9
26.25	12.71	162.2	7.3	105.4	7.5	56.8	1.6	14.3	1.1
28.25	14.00	101.5	6.1	41.0	6.3	60.5	1.5	8.0	0.9
29.75	15.10	83.8	5.6	31.4	5.7	52.4	1.2	1.8	0.7
31.25	16.14	85.5	5.8	32.8	6.0	52.7	1.3	2.7	0.7

TABLE 2 | ^{210}Pb chronology of Sky Pond (SKP) corresponding to **Figure 2**.

		Chronology					
Depth		Date	Age		Sedimentation rate		
cm	g cm^{-2}	AD	*y*	±	g cm^{-2} y^{-1}	cm y^{-1}	± (%)
0.00	0.00	2015	0.0	0			
0.25	0.06	2015	0.1	1	0.41	1.38	6.1
2.25	0.67	2013	1.6	2	0.42	1.32	6.8
4.25	1.33	2012	3.2	2	0.42	1.21	6.6
6.25	2.07	2010	4.9	2	0.39	1.00	7.2
8.25	2.89	2008	7.2	2	0.37	0.85	7.2
10.25	3.78	2005	9.6	2	0.37	0.74	6.3
12.25	4.89	2002	12.6	2	0.34	0.60	7.3
14.25	6.07	1999	16.3	2	0.27	0.46	7.1
16.25	7.20	1994	21.2	2	0.23	0.40	7.3
18.25	8.34	1989	26.4	2	0.22	0.37	9.6
20.25	9.50	1983	31.9	2	0.19	0.35	8.9
22.25	10.54	1977	38.0	3	0.17	0.32	11.2
24.25	11.55	1971	44.3	3	0.15	0.29	12.4
26.25	12.71	1963	52.0	4	0.14	0.19	15.4

changes) (Dekkers, 1997; Walden et al., 1999). The size, mineralogy and concentration of magnetic grains within SKP1 were characterised (**Figure 3** and **Supplementary Figures S2**, **S3**). χ_{LF}, values 0.3–0.43 10^{-6} m^3 kg^{-1} suggest a potential mix of ferrimagentic, antiferromagnetic, and diamagnetic grains (Walden et al., 1999), typical of mixed mineral assemblages, characteristic of lake sediments. Fine-grained (stable domain, ∼0.1–20 μm) magnetite dominates throughout the core, with a small antiferromagnetic component, indicated by S-RATIOs -0.6 to −0.7 (Robinson, 1986; Robertson et al., 2003; Hatfield, 2014) and supported by SIRM/χ_{LF} values < 22 k Am^{-1} which excludes significant contribution of authigenic iron sulphides (pyrite or greigite) (Thompson, 1980; Maher and Thompson, 1999) indicative of post-depositional changes due to reducing environments within the pond (Dekkers, 1997). The presence of bacterial magnetosomes is also excluded by χ_{ARM}/SIRM values < 2 10^{-3} mA^{-1} (Oldfield, 2007).

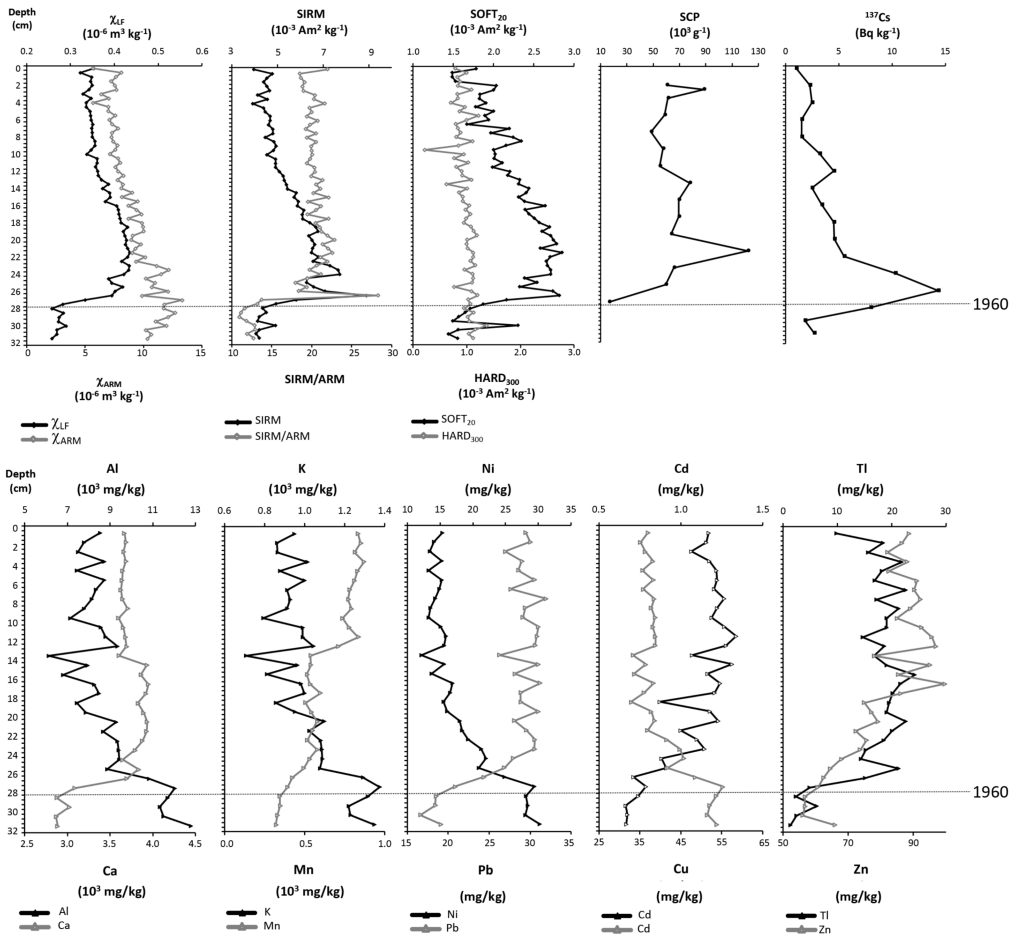

FIGURE 3 | Down-core concentrations of selected geomagnetic parameters, ^{137}Cs, elements and SCPs for Sky Pond (SKP1), showing the basal layer at ∼1960.

The contribution of sediment from land surrounding the pond is expected to be minimal due to the negligible catchment areas as defined by the stone and concrete margins. This is confirmed by χ_{FD} values ∼1–4% highlighting the minimal presence of superparamagnetic (<0.02 μm) grains, characteristic of catchment-derived eroded soil particles (Dearing et al., 1996). Furthermore, the deposition of Al, a tracer for minerogenic inputs, is independent to the typically anthropogenic heavy metals Pb, Zn, and Tl, as revealed by down-core concentration trends (**Figure 3**) and a lack of statistical association between Al and these metals (**Supplementary Tables S1**, **S2**).

DISCUSSION

Anthropogenic Signals in SKP

Changes in the magnetic and geochemical concentrations at SKP are not governed by catchment or post-depositional processes, therefore atmospheric deposition is the likely dominating source of magnetic grains in SKP sediments. Anthropogenic magnetic grains include combustion-derived magnetite nanoparticles (Maher et al., 2016), fine iron spherules (<3 μm) and coarse magnetite grains derived from road traffic (Matzka and Maher, 1999; Robertson et al., 2003; Blaha et al., 2008; Maher et al., 2008) and industry (Yang et al., 2010; Magiera et al., 2012), with characteristic antiferromagnetic (>2 μm) spheres from coal combustion and heavy industries (Oldfield, 2014).

Spheroidal carbonaceous particles are unambiguous indicators of fossil fuel combustion (Rose et al., 2004; Momose et al., 2012) and are ubiquitous in SKP sediments (16,140 g^{-1}–121,886 g^{-1}). Concentrations are higher by an order of magnitude to maximum SCP concentrations reported for other Chinese lakes (Rose et al., 1999, 2004; Wu, 2005; Panizzo et al., 2013; Zeng et al., 2015). For example, maximum SCP concentrations of ∼10,000 g^{-1} (at 1996) were measured in lake sediments from Hubei Province with surrounding mining and smelting industries (Zeng et al., 2015). This potentially highlights a comparatively raised level of contamination experienced at SKP and also suggests that the geography of SKP is crucial for the trapping and retention of particulate pollution due to its size, elevation and proximity to two coal fired power stations; Luohuang Power Station that has been operational since 1991

(∼12 km southeast of SKP) and Chongqing Power Station, built in 1952 (∼15 km northeast of SKP).

Enrichment factors are typically used to assess the anthropogenic contribution to total metal concentrations in lake sediments (Hilton et al., 1986) using a reference material for background crustal abundance or pre-industrial element concentrations. SKP has a sediment record that only reliably extends to 1961 and, therefore, does not provide baseline geochemical concentrations from 'pre-industrial' sediments (i.e., before the establishment of the People's Republic of China in 1949). Therefore, a geoaccumulation index (I_{geo}) (Muller, 1969) was applied to evaluate the extent of anthropogenic metal contamination within the pond sediments (**Table 3**) calculated by:

$$I_{geo} = \log_2\left(\frac{C_n}{1.5B_n}\right)$$

Where C_n is the measured concentration of nth element within the pond sediments and B_n is the referenced geochemical background value. The 1.5 constant normalises for geological variations. Available geochemical data for Chinese crustal material, national soils and local (Chongqing) soils are applied as a proxy for natural, geogenic inputs. However, due to the rapid industrialisation experienced in China throughout the 20th century, surface soil values are likely to be contaminated by anthropogenic emissions (Muller, 1969; Cheng et al., 2014).

Mean element concentrations measured in SKP1 sediments are presented (**Table 3**) alongside available mean background geochemical data for uncontaminated urban soils in Chongqing (analysed at a depth of 150–200 cm) (Cheng et al., 2014) national soils (Cheng et al., 2014) and crustal abundance (Tong, 1995; Min et al., 2014). Concentrations of Cr, Co, Mn, and Ni in SKP do not exceed background values (**Table 3**), suggesting they are derived from the local geology. This is supported by Cheng et al. (2014) who report relatively higher concentrations of Cr and Ni in deep (pre-industrial soils) compared to surface soils in Chongqing.

Mean Cd (1.141 mg/kg) and Tl (18.539 mg/kg) concentrations measured in SKP sediments are elevated above the crustal abundance baseline values: 0.055 and 0.610 mg/kg, respectively (**Table 3**). Mean I_{geo} values for Cd normalised for crustal abundance (3.8) indicate that the sediments are heavily contaminated, and Tl mean I_{geo} values (4.3) suggest heavy to extreme contamination (**Table 3**). Elevated levels of Cd, have also been reported in surface soils of Chongqing (Cheng et al., 2014) and excessive loadings of Cd (3.01 × greater than background values) were recorded in soils from Tonghan, Tongliang, Hechuan, and Dazu in west Chongqing (Jia et al., 2018). This confirms a Cd-enriched pollution signal, potentially reflecting smelting emissions (Jarup, 2003) and/or coal combustion since coal in Chongqing is highly enriched in Cd (Shi et al., 2018). Atmospheric Tl is likely to derive from fly ash from coal combustion, cement production or metallurgical industries (Karbowska, 2016). Pb, Zn, and

TABLE 3 | Mean, maximum and minimum geochemical concentrations (mg/kg) measured in SKP1 with corresponding background mean concentrations (mg/kg), where available, for urban soils in Chongqing (Cheng et al., 2014; Jia et al., 2018), Chinese soil background (Teng et al., 2014) and Chinese continental crustal abundance (Tong, 1995; Min et al., 2014).

	SKP geochemical concentrations (mg/kg)			Background reference material geochemical concentrations (mg/kg)			Mean I_{geo} values for SKP1		
Element	**Mean**	**Minimum**	**Maximum**	**Chongqing deep urban soil**	**National soil background**	**National crustal abundance**	I_{geo} **Chongqing soils**	I_{geo} **national soil**	I_{geo} **national crustal**
Al	8346	6126	10818		(6.6%)	74500			
Ba	82	69	104		469	610		*−3.1*	*−3.5*
Ca	3749	3596	3946		(15%)	43200			
Cd	1.14	0.71	1.34	0.12	0.10	0.06	***3.2***	***2.9***	***3.8***
Co	15	12	18	14.98	13	32	*−0.6*	*−0.4*	*−1.7*
Cr	21	16	25	80	61	63	*−2.0*	*−2.2*	*−2.2*
Cu	38	33	48	27	23	38	***0.5***	***0.14***	*−0.6*
Fe	20205	16104	23402		(3.0%)	50800			
K	968	708	1290		(1.9%)	23400			
Mg	1386	1159	1817		(0.78%)	21500			
Mn	661	424	870	569.1	582	780	*−0.4*	*−0.4*	*−0.9*
Na	61	43	86		(1.0%)	23600			
Ni	17	11	27	32	27	57	*−1.0*	*−1.3*	*−2.4*
Pb	29	24	32	26	27	15	***0.2***	*−0.3*	***0.4***
Tl	18.54	9.85	24.19		0.62	0.61		***4.3***	***4.3***
Zn	83	62	100	82	74	86	*0.0*	*−0.4*	*−0.6*

Mean geo-accumulation index (I_{geo}) values for SKP (italicised) were normalised using the background reference values. Extent of anthropogenic contamination is indicated by I_{geo} values: <0: uncontaminated; 0 ≤ 1: low to moderate contamination; 1 ≤ 2: moderate contamination; 2 ≤ 3: moderate to heavy contamination; 3 ≤ 4: heavily contaminated; 4 ≤ 5 heavily to extremely contaminated; and >5: extremely contaminated (Muller, 1969). Bold values highlight contamination detected in SKP sediment.

Cu exhibit relatively low contamination or uncontaminated levels.

To further determine anthropogenic sources, synchronicity in the deposition of SCPs, elements and magnetic grains in SKP sediments were investigated by principle component analysis (PCA) (**Table 4** and **Supplementary Table S1**) of the correlation coefficients between variables (**Supplementary Table S2**). Principle components (PC) PC1, PC2, and PC3 explain 80.52% of the total variance of the data (**Table 4**). Loading scores for PC1 and PC2; and PC1 and PC3 are plotted (**Figure 4**) to show mutuality between variables, supported by identified clusters within the PCA (**Supplementary Table S1**).

PC1 has positive loadings (>0.5) on SIRM, $HARD_{300}$, Al, Ba, Co, Cr, Cu, Fe, K, Mg, and Ni. This potentially reflects a minerogenic or catchment derived source as K and Al are major constituents of silicate minerals (Ma et al., 2016). This is supported by the low I_{geo} values for Ni, Co, and Cr and the identification of a natural origin of K, Fe, and Ba in modern atmospheric particulate samples from Chongqing (Chen et al., 2017).

PC2 demonstrates positive strong loadings with χ_{LF}, $SOFT_{20}$, and Ca, and moderate loadings for SCPs, SIRM, and Tl. Cluster analysis shows that this group is most represented by SIRM (**Supplementary Table S1**). The magnetic parameters reflect a mixture of anthropogenic and geogenic inputs, however, the lack of statistical correlation observed between the magnetic parameters and Fe (**Supplementary Table S2**), indicates an overriding anthropogenic magnetic signal (Yunginger et al., 2018). Some Ca is likely to derive from the surrounding limestone ($CaCO_3$) geology; however, the loading of Ca on PC2 instead of the minerogenic PC1 and strong correlations with SIRM, $SOFT_{20}$, and χ_{LF}, highlight an anthropogenic source. Calcium-rich dust from cement plants, mining activities and construction (Magiera et al., 2012; Khatri and Tyagi, 2014) are potential sources as well as calcite fly ash from Luohuang Power station as reported by Liu et al. (2016). Moderate loadings of SCPs and Tl on PC2 suggest that high Tl contamination (revealed by I_{geo} values > 4) is derived from coal combustion (Xiaoyan et al., 2015). PC3 is characterised by Cd, Pb and Zn, indicating a mutual anthropogenic source of these metals.

TABLE 4 | Principle component analysis (PCA) for SKP1 showing loadings of variables on the principle components (PC), eigenvalues, the percentage of variance of total sample explained by the PC and cumulative variance.

	PC1	PC2	PC3	PC4
χ_{LF}	0.37	**0.86**	0.18	−0.11
SIRM	*0.65*	*0.67*	−0.01	−0.10
$SOFT_{20}$	0.45	**0.81**	−0.04	−0.11
$HARD_{300}$	*0.53*	0.45	−0.11	0.07
SCP	−0.29	*0.58*	0.48	−0.44
Al	**0.85**	−0.31	0.36	−0.03
Ba	**0.82**	−0.33	−0.01	0.16
Ca	0.32	**0.80**	0.31	0.23
Cd	*−0.60*	−0.01	**0.73**	−0.04
Co	**0.91**	−0.27	0.18	−0.10
Cr	**0.79**	*−0.41*	*0.40*	−0.03
Cu	**0.86**	−0.35	0.06	−0.03
Fe	**0.86**	−0.25	0.40	−0.05
K	**0.90**	−0.19	0.32	0.10
Mg	**0.99**	−0.02	−0.04	0.03
Mn	*−0.61*	*−0.65*	0.32	−0.21
Na	−0.26	0.12	0.34	**0.85**
Ni	**0.99**	0.02	−0.01	0.03
Pb	−0.25	0.15	**0.78**	−0.13
Tl	−0.15	*0.57*	0.12	0.17
Zn	*−0.66*	−0.17	**0.64**	0.13
Eigenvalue	9.65	4.52	2.74	1.17
Variance (%)	45.95	21.51	13.07	5.58
Cumulative variance (%)	4.90	67.46	80.52	86.10

*Values highlighted in bold indicate strong loadings (>0.7) and italicised are moderate loadings (0.5–0.7). PCA produced four PCs with eignvalues > 1, the first two (PC1 and PC2) are plotted to show the mutual correlations between variables (**Figure 4**).*

A History of Air Pollution Deposition in Chongqing

The relatively high sediment accumulation in recent SKP sediments (**Figure 2D**) may result in a diluting effect on metal enrichment (Boyle et al., 1999; Yao and Xue, 2013). Therefore, geomagnetic, geochemical and SCP concentrations have been converted to flux (sediment accumulation) profiles (Norton et al., 1992; Vesely et al., 1993; Han et al., 2015) to show more accurately the deposition of magnetic grains, metals and pollution particles over time (**Figure 5**).

The SKP sediment record encompasses a time of extensive urban development in Chongqing, reflected by enhancements in magnetic grains, SCPs, Ca and metals post-1960. Three distinct temporal phases of pollution deposition are identified, coinciding with key phases in the urban history of Chongqing:

Phase I: 1960–1980 (21–28 cm) is characterised by relatively low supply of magnetic grains, SCPs, Ca and metals, reflecting a time of comparatively low environmental pollution. The SCP, magnetic and metal flux profiles exhibit slight increases post-1960, however, only Ca exhibits minimal values, increasing steadily from 1970.

Industry had already established and intensified in Chongqing at this time, with low-scale industries such as match making, silk reeling and cotton textiles occurring since the late 19th century. Ordnance industry, iron and steel works, and machinery manufacturing occur during the late 1930s. The Chongqing Special Steel Company was established in 1934, located 12 km northeast of SKP. Heavy industries, large scale manufacturing, coal fired power stations and electricity generation, followed the establishment of the People's Republic of China in 1949. Further industrial expansion occurred post-1963, as military-related industries, including weapons manufacturing, shipbuilding, space and aeronautics and metallurgy activities, located to Chongqing.

Phase II: 1980–1997 (14.5–21 cm) exhibits steadily increasing trends in SIRM, $SOFT_{20}$, SCPs, Ca, Cd, Pb, Tl, and Zn flux. $HARD_{300}$ remains relatively consistent.

Pollution increases throughout this phase reflect further industrial diversification including car manufacturing,

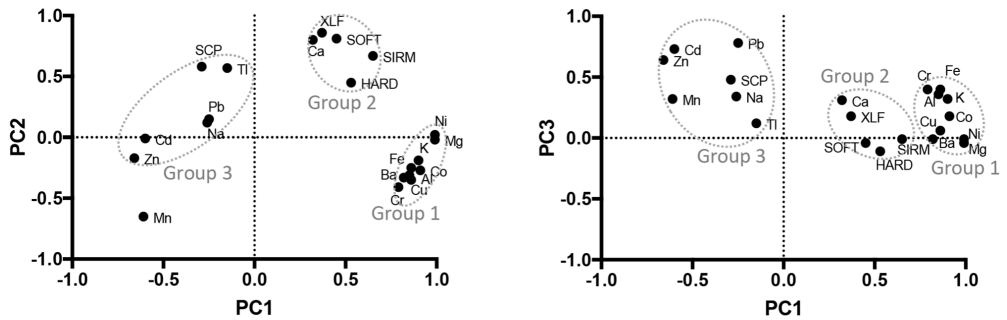

FIGURE 4 | Principle component analysis of magnetic, SCP and element concentration data for SKP1. Loading scores for principle components (PC) PC1 and PC2; and PC1 and PC3 (**Table 4**) are plotted. The proximity of variables corresponds to the strength of their mutual correlation.

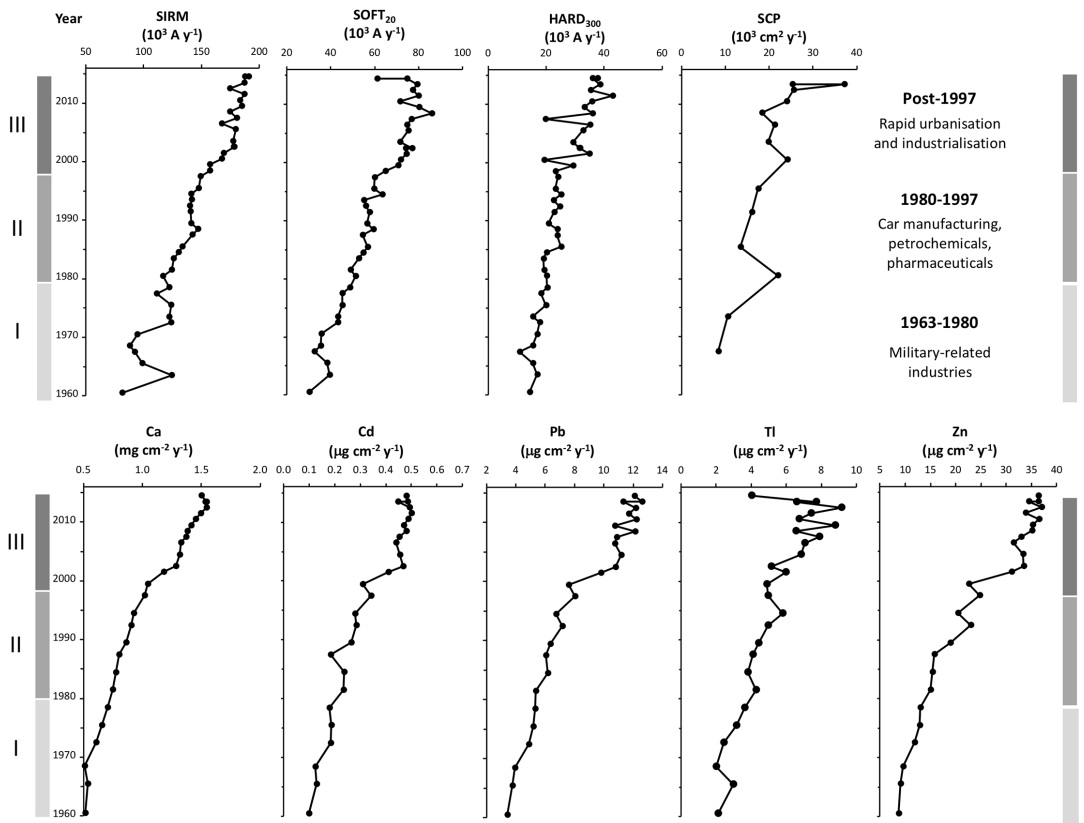

FIGURE 5 | Flux profiles for Sky Pond (SKP1) showing deposition of magnetic grains (SIRM, $SOFT_{20}$, and $HARD_{300}$), SCPs and identified anthropogenic geochemical tracers: Ca, Cd, Pb, Tl, and Zn. Superimposed are distinct phases identified from the flux profiles, which relate to the urban history of Chongqing.

petrochemicals and pharmaceuticals that occurred post-1981 (Liu, 2008). Chongqing became one of the fastest growing industrial centres in China during the late 20th century. A likely source of SCPs contributing to the prominent increasing trend ∼post-1950 is Chongqing Power Station, constructed in 1952.

Phase III: post-1997 (0–14.5 cm). Prominent increases are observed in SIRM, $SOFT_{20}$, $HARD_{300}$, SCPs, and metals, reaching maximum flux for SCPs in recent sediments (2013), SIRM (2013), $SOFT_{20}$ (2008), $HARD_{300}$ (2013), Ca (2009), Cd (2011), Pb (2014), Tl (2012), and Zn (2012).

Notable pollution enrichment in this most recent section of the core coincides with rapid urbanisation and industrialisation post-1997, when Chongqing was designated one of four municipalities directly controlled by central government. Chongqing became a prominent megacity, experiencing urban expansion, extensive construction, improvements in

transport infrastructure, rise in private car use and population increases. The urban population rose from 17.9% of the total population of Chongqing in 1978 to 51.3% in 2011 (Cheng et al., 2014). Chongqing developed into a major manufacturing centre for automobiles, steels, aluminium and chemicals. In 1995 Chongqing Iron and Steel Company expanded its manufacturing capacities in Daduko. Intense economic growth was fuelled by coal combustion. Also, in 1995 Chongqing Power Station increased its capacity from 200 to 800 MW and Luohuang Power Station, operational post 1991 (2 × 360 MW), doubled its capacity in 1998 and further expanded in 2006.

The consumption of fuel in Chongqing has increased steadily since 1949 from <880,000 tonnes to 44,645,800 tonnes in 2005, with more prominent increases into the 21st century (89,197,400 tonnes in 2013) (**Figure 6**). In 1949 coal represented 97% of fuel consumed, however, in 2013 this value had dropped to 66.5% due to increased use of oil, which comprised only 2.2% of energy used in 1949 but increased to 11.6% in 2013; and natural gas which has increased from 1.3% in 1957 to 10.7% in 2013 (Fumin and Zesheng, 2016). Temporal agreement and strong positive correlations observed between SIRM, Tl, Cd, and SCP flux and historical fuel consumption trends for Chongqing (**Figure 6** and **Table 5**) provide further evidence that a robust history of air pollution relating to regional industrial and urban development has been achieved for SKP. Identifying specific pollutant sources to SKP is difficult due to the complex nature of urban pollution, however, an overriding pollution signal from fossil fuel combustion is supported by Chen et al. (2017) who report that coal and vehicle emissions are the primary cause of contemporary $PM_{2.5}$ pollution in Chongqing.

Comparison of Air Pollution Histories From Chongqing and Merseyside

The deposition of SCPs in natural archives has been used as a global stratigraphic marker to determine the onset of the Anthropocene, revealed by rapid increases in concentrations post-1950 (Swindles et al., 2015). Sediment archives from the United Kingdom typically exhibit peak SCP concentrations from 1970 to 1980, with regional variations (Rose and Appleby, 2005); however, urban ponds that are sensitive to changes within the urban landscape, are rarely used in environmental reconstructions. We present an air pollution record from a small urban pond, Dogs Kennel Clump (DKC) in Merseyside, northwest England, as a comparative example of urban air pollution in the United Kingdom. An industrial heartland of Britain, the Merseyside region has experienced progressive industrialisation since the early 19th century, characterised by chemicals production, oil refineries, car manufacturing and power generation, with intense urbanisation since the mid 20th century.

A high-resolution, localised history of urban air pollution has been achieved from DKC. Full radiometric (**Supplementary Figures S4**, **S5** and **Supplementary Tables S3**, **S4**), geomagnetic (**Supplementary Figures S6**, **S7**), and geochemical (**Supplementary Figure S8**) records are provided.

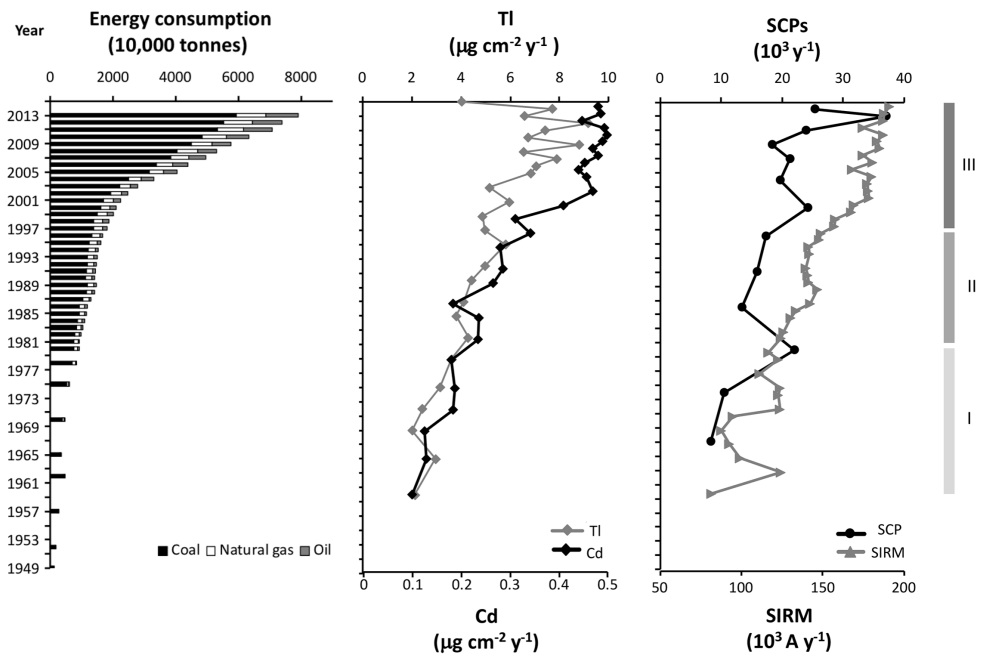

FIGURE 6 | Historical fuel consumption trends for Chongqing (Fumin and Zesheng, 2016) showing coal, natural gas and oil consumption from 1949 to 2013, plotted alongside pollution flux data from SKP (1960–2015). SIRM, a proxy for PM_{10} and $PM_{2.5}$ pollution (Speak et al., 2012; Wang et al., 2017); SCPs, unambiguous indicator of fossil fuel combustion (Rose, 2015); Tl, a tracer for coal emissions (Vaněk et al., 2016) and smelting (Karbowska, 2016); and Cd, a tracer for industry, smelting and coal combustion (Gao et al., 2013; Shi et al., 2018) are presented. Tl and Cd were selected as metals representative of anthropogenic enrichment (**Table 3**). Flux trends mirror increases in coal, gas and oil consumption since 1960 and statistically significant correlations are observed (**Table 5**).

TABLE 5 | Correlations between consumption of total energy, coal, oil and natural gas in Chongqing (1949–2013; $n = 42$) and SKP flux data: SIRM ($n = 42$), SCPs ($n = 13$), Tl and Cd ($n = 27$) corresponding to **Figure 6**.

	Total energy consumption	Coal	Natural gas	Oil
Coal	0.999***			
Natural gas	0.998***	0.996***		
Oil	0.997***	0.995***	0.993***	
SCP flux	0.633*	0.624*	0.657*	0.634*
SIRM flux	0.934***	0.938***	0.939***	0.914***
Tl flux	0.923***	0.924***	0.930***	0.904***
Cd flux	0.935***	0.943***	0.937***	0.920***

*Significant relationships are shown as indicated by p-values: *$p < 0.05$, **$p < 0.005$, ***$p < 0.001$.*

Down-core variations in magnetic, SCP and metal flux are presented (**Figure 7**). Ba, Cu, Pb, and Zn, were determined as anthropogenically derived by PCA (**Supplementary Figure S9** and **Supplementary Table S6**) and significantly correlated to SCP deposition (**Supplementary Table S5**) indicating an atmospherically derived anthropogenic source. I_{geo} values for these elements (**Supplementary Table S7**) indicate DKC sediments are uncontaminated by Ba, low to moderately contaminated by Pb and Cu, and moderately to heavily contaminated by Zn. The pollution record achieved typifies pollution trends observed for the region determined by other urban ponds in the locality and exhibits three man phases of pollution deposition relating to localised urban activity (**Figure 7**):

Phase I: 1910–1950 (34–51 cm). Relatively low magnetic, trace metal and SCP flux. SCP increases are observed from 1930 and magnetic grains steadily increase.

Regionally, industry was established in the nearby City of Liverpool, and industrial towns of Widnes (<5 km east) and Runcorn (<4 km southeast), which experienced modernisation and diversification since the start of the 20th century. Runcorn and Widnes became major manufacturing centres for chemicals. Oil refineries and petrochemical industries were established at Ellesmere Port (∼8 km southwest) from 1920 and Speke Airport, a small airbase (<3 km west) opened in 1930.

Phase II: 1950–1990 (22.5–34 cm). Metals, magnetic grains and SCP flux steadily increase, with distinct Zn enhancement.

Zn increases coincide with the introduction of local industries at Halewood (<3 km northwest) including pharmaceuticals, chemicals, foundries and concrete works. Further enhancement in Zn during the 1960s reflects the establishment of a major car manufacturing plant in 1963. Industry continued to diversify and intensify in the Merseyside region and three coal-fired power stations opened: Ince Power Station (240 MW capacity) in 1957, Bold Power Station (300 MW capacity) in 1958 and Fiddlers Ferry Power Station (2000 MW capacity) in 1973 (**Figure 1**). Localised urban expansion occurred throughout this phase, with residential developments in Halewood, resulting in a 10-fold increase in the local population. Motorways were constructed locally and road transport increased. During the mid-20th century, nation-wide air quality legislations were established, such as the Clean Air Acts (1956, 1964), reducing national domestic coal combustion, followed by the Control of Pollution Act (1975), Motor Fuel Regulations (1981) and the Environmental Protection Act (1990). Leaded petrol started to be phased out with the introduction of unleaded petrol in 1988.

Phase III: post-1990 (0–22.5 cm). Further pollution enhancement reaching peaks at ∼2000. Subsequent overall steady declines in SCPs, metals and magnetic grains are observed, however, magnetic and metal flux remain elevated above pre-1990 levels.

Continued urbanisation in the region occurred, including the expansion of Liverpool John Lennon International Airport (formerly Speke Airport) with increased air and road transport. Ince and Bold coal fired power stations closed in 1997 and 1991, respectively. Stringent air quality legislations (EU Air Quality Framework Directives, 1996 and United Kingdom Air Quality Strategy, 1997) were introduced and periodically revised.

Tl and Cd concentrations were below detectable levels in DKC sediment. In contrast, the observed anthropogenic enrichment of these metals in SKP, further strengthens an important regional, Cd and Tl-rich signature of air pollution in Chongqing. The relative importance of coal as a dominating pollution source for Chongqing is further supported by mean post-1997 SCP flux values of 24.418 10^3 y^{-1} for SKP, compared to relatively lower values: 10.266 10^3 y^{-1} for DKC. Peak SCP flux occurs at 2001 in DKC (maximum 17.116 10^3 y^{-1}) after which, steadily declining flux trends, reflect the reduced consumption of coal in the United Kingdom, local coal fired power station closures and effective pollution controls.

Industrialisation post-1960 in Chongqing mirrors the United Kingdom experience during the United Kingdom 'Great Acceleration' during the early 20th century. Maximum magnetic, SCP, Ba, Cu, Pb, and Zn flux values occur at ∼2000 at DKC. Despite national attempts to reduce air pollution, extending back to 1956 in the United Kingdom with the introduction of the Clean Air Act and subsequent, increasingly stringent legislations, it is not until post-2001 that a steady reduction in pollutants is observed at DKC. Furthermore, pollution levels do not decrease to below ∼pre-1990 levels. The reduction in Pb post-2000 reflects the United Kingdom ban of tetraethyl lead in 1999.

Whereas in the United Kingdom, clean air quality controls were influential, similar reductions in pollution are not observed in SKP. In China, air pollution is currently addressed through the consumption of less polluting fuels, including a nation-wide ban on leaded petrol during the early 2000s, improved urban planning, the relocation of industries, zoning regulations (Kan et al., 2012) and recently, the construction of air purifying towers (Lewis, 2018). The lack of pollution reduction in the SKP sediments reveal that, despite the introduction of air quality legislations in China since 1982 and tightened controls in 1996 with the establishment of the National Standard, the anticipated reductions in overall atmospheric pollution have been overwhelmed and offset by the intensity of urban development.

A key characteristic of the air pollution record achieved at DKC, is a shift to a relatively fine magnetic signal in post-1990 sediments, revealed by proportionately higher χ_{ARM} concentrations compared to χ_{LF} (**Figure 8**). Further magnetic

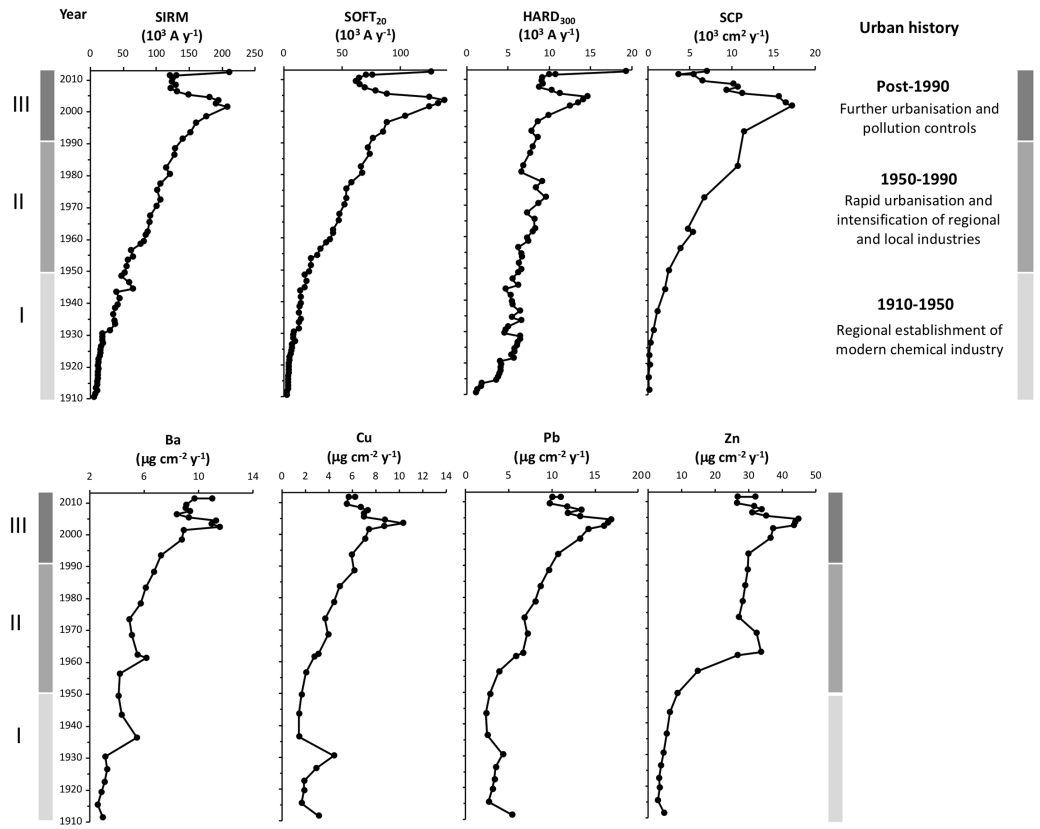

FIGURE 7 | Flux profiles for Dogs Kennel Clump Pond (DKC) showing deposition of magnetic grains (SIRM, $SOFT_{20}$, and $HARD_{300}$), SCPs and identified anthropogenic geochemical tracers Ba, Cu, Pb, and Zn. Superimposed are distinct phases identified from the flux profiles, which relate to the urban history of the Merseyside region.

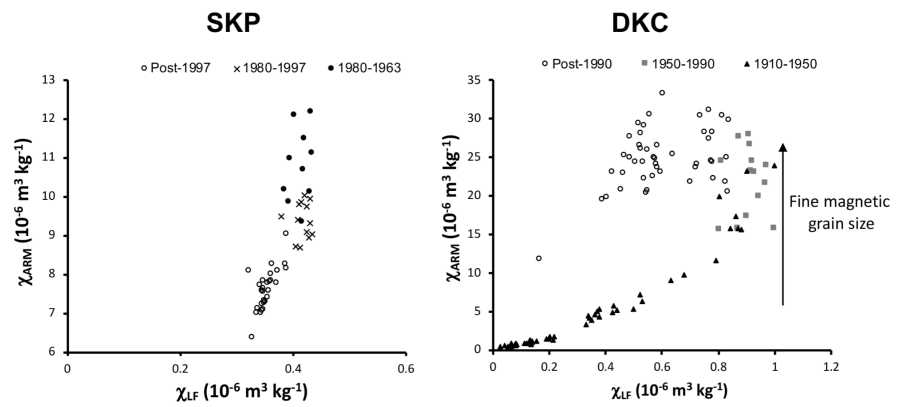

FIGURE 8 | Temporal changes in ferrimagentic grain size indicated by χ_{LF} versus χ_{ARM} (after King et al., 1982) for SKP and DKC. Distinct temporal phases identified from the magnetic flux profiles are shown for SKP (1963–1980, 1980–1997 and post-1997) and for DKC (1900–1950, 1950–1990 and post-1990). Shifts in relative grain size variations are determined since χ_{ARM} values are sensitive to the contribution of single stable domain (SSD) and pseudo stable domains (PSD), with a physical grain size < 2 µm. χ_{LF} reflect the concentration of total ferrimagentic grains. Linear increases are indicative of increasing magnetic concentration, however, steeper slopes as shown, indicate finer ferrimagnetic grain size assemblages.

characterisation (**Supplementary Figure S7**) reveals this increase in fine magnetic grains is typical of urban combustion dusts. Road and air travel are potentially important sources of combustion particles post-1990, due to increased transportation trends and the proximity of DKC to Liverpool John Lennon International Airport, an important transport hub for the region. DKC reveals that although air quality controls may be reducing the release of coarse pollution particles, as indicated by post-2000

pollution declines, a finer, and therefore, potentially more toxic (Chow et al., 2006; Pope and Dockery, 2006; Pope et al., 2015) combustion-derived pollution signal has increased since the 1990s.

In contrast, SKP exhibits a coarsening of the magnetic signal in post-1997 sediments (**Figure 8**). This potentially highlights a recent, localised effect of pollution captured by SKP as urban expansion has occurred over time, since the size of particle deposition increases with proximity to pollution source (Inoue et al., 2013). Furthermore, increased coal combustion from Chongqing and Luohuang Power Stations are likely sources of coarse magnetic grains (Locke and Bertine, 1986).

Historical Air Pollution Exposure in Chongqing

The sediments of SKP identify a history of increasing metal pollution in Chongqing since 1960, with notable enhancement in Zn, Pb, Cd, Tl, and Ca post-1997, revealing the changing levels of harmful atmospheric contaminants in Chongqing, over time. Comparisons of mean geochemical flux data reveal that compared to 1960–1980 (Phase I), the population of Chongqing potentially experienced 3.098 × higher Zn, 3.035 × higher Cd, 2.525 higher Pb, and 2.493 × higher Tl levels during 1997–2015 (Phase III). This suggests that as urban populations have increased in Chongqing they have also been exposed to higher pollution levels, compared to previous generations.

Tl is highly toxic at low concentrations (Karbowska, 2016), more toxic than Hg, Cd, Pb, or Zn and acute exposure affects the nervous system, lungs, heart, and kidneys and can be fatal (Peter and Viraraghavan, 2005). Cd is toxic to the kidneys and can impair lung function and potentially lead to lung cancer (Cheng et al., 2016). Pb is classified as a probable carcinogen affecting neurological development in children (Lidsky and Schneider, 2003) and Zn can affect the pulmonary stem when inhaled (Chen and Lippmann, 2009; Roney et al., 2016). SIRM flux, a proxy for total metals and PM_{10} deposition (Mitchell and Maher, 2009; Speak et al., 2012), highlights the continued release of PM since the 1960s to present day in Chongqing. PM_{10} and $PM_{2.5}$ have been linked to various diseases including childhood asthma (Brugha and Grigg, 2014), chronic obstructive pulmonary disease (COPD) (Andersen et al., 2011; Postma and Rabe, 2015), heart disease (Beelen et al., 2014), stroke (Pope et al., 2015), neurodegenerative diseases, such as dementia (Maher et al., 2016), cancers (Wong et al., 2014) and premature mortality (Anenberg et al., 2010).

Our understanding of the long-term health effects from chronic air pollution exposure is limited due to lack of historical air quality data. Determining relationships between public health and the environment are complex, since exposure pathways include inhalation, dermal contact and ingestion, further complicated by health implications of lifestyle factors, genetics, and occupation; the cumulative exposure to atmospheric contaminants for urban populations is an important consideration. This is especially crucial for the population of Chongqing, where the air pollution record from SKP reveals long-term, increasing releases of PM, highly contaminated with Cd and Tl.

Stratigraphic markers of industrialisation such a heavy metals, SCPs and radioactive isotopes in environmental archives are commonly used to assign a precise date to the global impact of human activity on the Earth system, marking the onset of the 'Anthropocene.' We show how these pollution tracers, deposited in urban pond sediments can reconstruct city-specific air pollution histories, enabling the exploration of how the nature of PM has changed throughout the 20th century. These pollution records allow us to assess how the releases of environmental toxins have changed over time, and identify how such changes may be related to intense urban and industrial expansions. These data demonstrate the efficacy of pollution controls and, perhaps most importantly, help determine potential life-time pollutant exposure in urban populations. This is crucial for understanding long-term health implications of air pollution and to protect human health in the future.

AUTHOR CONTRIBUTIONS

AP, RT, RJ, JD, YT, AW, and JL contributed to conception and design of study, collected samples, and edited the manuscript. AP, AW, and JD analysed and interpreted data. AP performed statistical analysis, constructed figures, and wrote the first draught of the manuscript. AW and JL wrote sections of the manuscript. All authors contributed to manuscript revision, read and approved the submitted version.

FUNDING

This research was supported by Halton Primary Care Trust (grant number CHCRD001 SE02), Edge Hill University (fund codes: RDWOR04, RDWOR05, RDWOR06, and RDWOR209), and the University of Exeter.

ACKNOWLEDGMENTS

We are grateful to Peter Appleby (Liverpool University Environmental Radioactive Laboratory) for radiometric dating analysis, Joana Zaragoza-Castells and Ange Elliott (University of Exeter, Geography Analytical Laboratories) for technical assistance, Naomi Edwards, Nia Glover, and Tim Brown for assistance with geomagnetic and geochemical analyses and Paul Fryer for map creation. This work is dedicated to the memory of our excellent colleague and dear friend Dr. Richard Jones (1972–2018).

SUPPLEMENTARY MATERIAL

The Supplementary Material for this article can be found online at: https://www.frontiersin.org/articles/10.3389/feart.2018.00131/full#supplementary-material

REFERENCES

Andersen, Z. J., Hvidberg, M., Jensen, S. S., Ketzel, M., Loft, S., Sørensen, M., et al. (2011). Chronic obstructive pulmonary disease and long-term exposure to traffic-related air pollution. *Am. J. Respir. Crit. Care Med.* 183, 455–461. doi: 10.1164/rccm.201006-0937OC

Anenberg, S. C., Horowitz, L. W., Tong, D. Q., and West, J. J. (2010). An estimate of the global burden of anthropogenic ozone and fine particulate matter on premature human mortality using atmospheric modeling. *Environ. Health Perspect.* 118, 1189–1195. doi: 10.1289/ehp.0901220

Appleby, P. G. (1992). Self-absorption corrections km well-type germanium detector. *Nucl. Instrum. Methods Phys. Res. B* 71, 228–233. doi: 10.1016/0168-583X(92)95328-O

Appleby, P. G., Nolan, P. J., Gifford, D. W., Godfrey, M. J., Oldfield, F., Anderson, N. J., et al. (1986). Pb-210 dating by low background gamma-counting. *Hydrobiologia* 143, 21–27. doi: 10.1007/BF00026640

Appleby, P. G., and Oldfield, F. (1978). The calculation of lead-210 dates assuming a constant rate of supply of unsupported 210Pb to the sediment. *Catena* 5, 1–8. doi: 10.1016/S0341-8162(78)80002-2

Beelen, R., Stafoggia, M., Raaschou-Nielsen, O., Andersen, Z. J., Xun, W. W., Katsouyanni, K., et al. (2014). Long-term exposure to air pollution and cardiovascular mortality: an analysis of 22 European cohorts. *Epidemiology* 25, 368–378. doi: 10.1097/EDE.0000000000000076

Bell, M. L., Davis, D. L., and Fletcher, T. (2003). A retrospective assessment of mortality from the london smog episode of 1952: the role of influenza and pollution. *Environ. Health Perspect.* 112, 6–8. doi: 10.1289/ehp.6539

Blaha, U., Sapkota, B., Appel, E., Stanjek, H., and Rösler, W. (2008). Micro-scale grain-size analysis and magnetic properties of coal-fired power plant fly ash and its relevance for environmental magnetic pollution studies. *Atmos. Environ.* 42, 8359–8370. doi: 10.1016/j.atmosenv.2008.07.051

Boyle, J. F., Rose, N. L., Bennion, H., Yang, H., and Appleby, P. G. (1999). Environmental impacts in the jianghan plain: evidence from lakes sdiments. *Water Air Soil Pollut.* 112, 21–40. doi: 10.1023/A:1005040713678

BP (2017). *BP Statistical Review of World Energy June 2016*. London: BP plc.

Brimblecombe, P. (2005). The globalization of local air pollution. *Globalizations* 2, 429–441. doi: 10.1080/14747730500368114

Brugha, R., and Grigg, J. (2014). Urban air pollution and respiratory infections. *Paediatr. Respir. Rev.* 15, 194–199. doi: 10.1016/j.prrv.2014.03.001

Brugha, R. E., Mushtaq, N., Round, T., Gadhvi, D. H., Dundas, I., Gaillard, E., et al. (2014). Carbon in airway macrophages from children with asthma. *Thorax* 69, 654–659. doi: 10.1136/thoraxjnl-2013-204734

Cao, J., Yang, C., Li, J., Chen, R., Chen, B., Gu, D., et al. (2011). Association between long-term exposure to outdoor air pollution and mortality in China: a cohort study. *J. Hazard. Mater.* 186, 1594–1600. doi: 10.1016/j.jhazmat.2010.12.036

Carbon Brief (2015). *UK Coal Use to Fall to Lowest Level Since Industrial Revolution*. Available at: https://www.carbonbrief.org/uk-coal-use-to-fall-to-lowest-level-since-industrial-revolution [accessed June 28, 2017]

Chang, S., Zhuo, J., Meng, S., Qin, S., and Yao, Q. (2016). Clean coal technologies in China: current status and future perspectives. *Engineering* 2, 447–459. doi: 10.1016/J.ENG.2016.04.015

Chen, K.-L., Wu, H.-N., Chengs, W.-C., Zhang, Z., and Chen, J. (2016). Geological characteristics of strata in Chongqing, China, and mitigation of the environmental impacts of tunneling-induced geo-hazards. *Environ. Earth Sci.* 76, 1–16.

Chen, L. C., and Lippmann, M. (2009). Effects of metals within ambient air particulate matter (PM) on human health. *Inhal. Toxicol.* 21, 1–31. doi: 10.1080/08958370802105405

Chen, Y., and Xie, S.-D. (2013). Long-term trends and characteristics of visibility in two megacities in southwest China: Chengdu and Chongqing. *J. Air Waste Manag. Assoc.* 63, 1058–1069. doi: 10.1080/10962247.2013.791348

Chen, Y., Xie, S.-D., Bin Luo, and Zhai, C.-Z. (2017). Particulate pollution in urban Chongqing of southwest China: historical trends of variation, chemical characteristics and source apportionment. *Sci. Total Environ.* 584–585, 523–534. doi: 10.1016/j.scitotenv.2017.01.060

Cheng, C., Xun, P., Nishijo, M., and He, K. (2016). Cadmium exposure and risk of lung cancer: a meta-analysis of cohort and case–control studies among general and occupational populations. *J. Expo. Sci. Environ. Epidemiol.* 26, 437–444. doi: 10.1038/jes.2016.6

Cheng, H., Li, M., Zhao, C., Li, K., Peng, M., Qin, A., et al. (2014). Overview of trace metals in the urban soil of 31 metropolises in China. *J. Geochem. Explor.* 139, 31–52. doi: 10.1016/j.gexplo.2013.08.012

Chow, J. C., Watson, J. G., Mauderly, J. L., Costa, D. L., Wyzga, E., Vedal, S., et al. (2006). Health effects of fine particulate air pollution: lines that connect. *J. Air Waste Manag. Assoc.* 56, 1368–1380.

Dearing, J. A., Hay, K. L., Baban, S. M. J., Huddleston, A. S., Wellington, E. M. H., and Loveland, P. J. (1996). Magnetic susceptibility of soil: an evaluation of conflicting theories using a national data set. *Geophs. J. Int.* 127, 728–734. doi: 10.1111/j.1365-246X.1996.tb04051.x

Dekkers, M. J. (1997). Environmental magnetism: an introduction. *Geol. Mijnbouw* 76, 163–182. doi: 10.1023/A:1003122305503

Fumin, Z., and Zesheng, T. (2016). *Chongqing Statistical Yearbook 2015*. Beijing: China Statistics Press.

Gao, B., Zhou, H., Liang, X., and Ti, X. (2013). Cd isotopes as a potential source tracer of metal pollution in river sediments. *Environ. Pollut.* 181, 340–343. doi: 10.1016/j.envpol.2013.05.048

Han, Y. M., Wei, C., Huang, R. J., Bandowe, B. A. M., Ho, S. S. H., Cao, J. J., et al. (2015). Reconstruction of atmospheric soot history in inland regions from lake sediments over the past 150 years. *Sci. Rep.* 6:19151. doi: 10.1038/srep19151

Hatfield, R. (2014). Particle size-specific magnetic measurements as a tool for enhancing our understanding of the bulk magnetic properties of sediments. *Minerals* 4, 758–787. doi: 10.3390/min4040758

Heiri, O., Lotter, A. F., and Lemcke, G. (2001). Loss on ignition as a method for estimating organic and carbonate content in sediments: reproducibility and comparability of results. *J. Paleolimnol.* 25, 101–110. doi: 10.1023/A:1008119611481

Hilton, J., Lishman, J. P., and Allen, P. V. (1986). The dominant processes of sediment distribution and focusing in a small, eutrophic, monomictic lake. *Limnol. Oceanogr.* 31, 125–133. doi: 10.4319/lo.1986.31.1.0125

Hunt, A. (1986). The application of mineral magnetic methods to atmospheric aerosol discrimination. *Phys. Earth Planet. Int.* 42, 10–21. doi: 10.1016/S0031-9201(86)80005-X

Inoue, J., Tomozawa, A., and Okudaira, T. (2013). The use of size distributions of spheroidal carbonaceous particles in swimming pool deposits for evaluating atmospheric particle behaviour. *Water Air Soil Pollut.* 224:1580. doi: 10.1007/s11270-013-1580-7

Jarup, L. (2003). Hazards of heavy metal contamination. *Br. Med. Bull.* 68, 167–182. doi: 10.1093/bmb/ldg032

Jia, Z., Li, S., and Wang, L. (2018). Assessment of soil heavy metals for eco-environment and human health in a rapidly urbanization area of the upper Yangtze Basin. *Sci. Rep.* 8:3256. doi: 10.1038/s41598-018-21569-6

Kahuthu, A. (2006). Economic growth and environmental degradation in a global context. *Environ. Dev. Sustain.* 8, 55–68.

Kan, H., Chen, R., and Tong, S. (2012). Ambient air pollution, climate change, and population health in China. *Environ. Int.* 42, 10–19. doi: 10.1016/j.envint.2011.03.003

Karbowska, B. (2016). Presence of thallium in the environment: sources of contaminations, distribution and monitoring methods. *Environ. Monit. Assess.* 188:640. doi: 10.1007/s10661-016-5647-y

Khatri, N., and Tyagi, S. (2014). Influences of natural and anthropogenic factors on surface and groundwater quality in rural and urban areas. *Front. Life Sci.* 8, 23–39. doi: 10.1080/21553769.2014.933716

Kim, D., and Kim, S.-K. (2012). Comparing patterns of component loadings: principal component analysis (PCA) versus independent component analysis (ICA). in analyzing multivariate non-normal data. *Behav. Res. Methods* 44, 1239–1243. doi: 10.3758/s13428-012-0193-1

King, J., Banerjee, S. K., Marvin, J., and Özdemir, Ö. (1982). A comparison of different magnetic methods for determining the relative grain size of magnetite in natural materials: some results from lake sediments. *Earth Planet. Sci. Lett.* 59, 404–419. doi: 10.1016/0012-821X(82)90142-X

Klimberg, R., and McCullough, B. D. (2016). *Fundamentals of Predictive Analytics with JMP®*, 2nd Edn. Cary, NC: SAS Institute Inc.

Kulmala, M. (2015). China's choking cocktail. *Nature* 526, 497–499. doi: 10.1038/526497a

Landrigan, P. J., Fuller, R., Acosta, N. J. R., Adeyi, O., Arnold, R., Basu, N., et al. (2017). The lancet commission on pollution and health. *Lancet* 391, 462–512. doi: 10.1016/S0140-6736(17)32345-0

Lewis, A. (2018). Beware China's 'anti smog tower' and other plans to pull sir pollution from the air. *The Independent*. Available at: https://www.independent.co.uk/environment/beware-chinas-antismog-tower-and-other-plans-to-pull-pollution-from-the-air-a8179061.html [accessed February 1, 2018].

Lidsky, J. S., and Schneider, T. I. (2003). Lead neurotoxicity in children: basic mechanisms and clinical correlates. *Brain* 126, 5–19. doi: 10.1093/brain/awg014

Liu, F. Z. (2008). 30 years' fast industrial development in Chongqing. *Chongqing Econ.* 6, 55–58.

Liu, H., Sun, Q., Wang, B., Wang, P., and Zou, J. (2016). Morphology and composition of microspheres in fly ash from the luohuang power plat, chongqing, Southwestern China. *Minerals* 6:30. doi: 10.3390/min6020030

Liu, L. (2010). Made in China: cancer villages. *Environ. Sci. Policy Sustain. Dev.* 52, 8–21. doi: 10.1080/00139151003618118

Locke, G., and Bertine, K. K. (1986). Magnetite in sediments as an indicator of coal combustion. *Appl. Geochem.* 1, 345–356. doi: 10.1016/0883-2927(86)90020-X

Ma, L., Wu, J., Abuduwaili, J., and Liu, W. (2016). Geochemical responses to anthropogenic and natural influences in Ebinur lake sediments of arid northwest China. *PLoS One* 11:e155819. doi: 10.1371/journal.pone.0155819

Magiera, T., Gołuchowska, B., and Jabłońska, M. (2012). Technogenic magnetic particles in alkaline dusts from power and cement plants. *Water Air Soil Pollut.* 224, 1–17.

Maher, B. A., Ahmed, I. A. M., Karloukovski, V., MacLaren, D. A., Foulds, P. G., Allsop, D., et al. (2016). Magnetite pollution nanoparticles in the human brain. *Proc. Natl. Acad. Sci. U.S.A.* 113, 10797–10801. doi: 10.1073/pnas.1605941113

Maher, B. A., Moore, C., and Matzka, J. (2008). Spatial variation in vehicle-derived metal pollution identified by magnetic and elemental analysis of roadside tree leaves. *Atmos. Environ.* 42, 364–373. doi: 10.1016/j.atmosenv.2007.09.013

Maher, B. A., and Thompson, R. (1999). *Climates, Environments and Magnetism*. Cambridge: Cambrige University Press. doi: 10.1017/CBO9780511535635

Matzka, J., and Maher, B. A. (1999). Magnetic biomonitoring of roadside tree leaves: identification of spatial and temporal variations in vehicle-derived particulates. *Atmos. Environ.* 33, 4565–4569. doi: 10.1016/S1352-2310(99)00229-0

Min, L., Xiaohuan, X., Guiyi, X., Hangxin, C., Zhongfang, Y., Gouhua, Z., et al. (2014). National multi-purpose regional geochemical survey in China. *J. Geochem. Explor.* 139, 21–30. doi: 10.1016/j.gexplo.2013.06.002

Mitchell, R., and Maher, B. A. (2009). Evaluation and application of biomagnetic monitoring of traffic-derived particulate pollution. *Atmos. Environ.* 43, 2095–2103. doi: 10.1016/j.atmosenv.2009.01.042

Momose, A., Inoue, J., Murakami-Kitase, A., Okudaira, T., and Yoshikawa, S. (2012). Characteristic differences in the chemical composition of spheroidal carbonaceous particles in Japanese and Chinese cities. *Water Air Soil Pollut.* 223, 4761–4767. doi: 10.1007/s11270-012-1232-3

Muller, G. (1969). Index of geoaccumulation in sediments of the Rhine River. *GeoJournal* 2, 108–118.

Norton, S. A., Beinert, R. W. J., Binford, M. W., and Kahl, J. S. (1992). Stratigraphy of total metals in PIRLA sediment cores. *J. Paleolimnol.* 7, 191–214. doi: 10.1007/BF00181714

OCED (2018). *OCED Urban Policy Reviews: China 2015*. Available at: http://www.keepeek.com/Digital-Asset-Management/oecd/urban-rural-and-regional-development/oecd-urban-policy-reviews-china-2015_9789264230040-en#.WlchIrasM6g#page2 [accessed April 4, 2018].

Oldfield, F. (2007). Sources of fine-grained magnetic minerals in sediments: a problem revisited. *Holocene* 17, 1265–1271. doi: 10.1177/0959683607085135

Oldfield, F. (2014). Can the magnetic signatures from inorganic fly ash be used to mark the onset of the Anthropocene? *Anthropocene Rev.* 2, 3–13. doi: 10.1177/2053019614534402

Panizzo, V. N., Mackay, A. W., Rose, N. L., Rioual, P., and Len, M. J. (2013). Recent palaeolimnological change recorded in Lake Xiaolongwan, northeast China, Climatic versus anthropogenic forcing. *Quat. Int.* 290–291, 322-334.

Peter, A. L., and Viraraghavan, T. (2005). Thallium: a review of public health and environmental concerns. *Environ. Int.* 31, 493–501. doi: 10.1016/j.envint.2004.09.003

Pope, C. A. III, Burnett, R. T., Turner, M. C., Cohen, A., Krewski, D., Jerrett, M., et al. (2011). Lung cancer and cardiovascular disease mortality associated with ambient air pollution and cigarette smoke: shape of the exposure-response relationships. *Environ. Health Perspect.* 119, 1616–1621. doi: 10.1289/ehp.1103639

Pope, C. A. III, and Dockery, D. W. (2006). Health effects of fine particulate air pollution: lines that connect. *J. Air Waste Manag. Assoc.* 56, 709–742. doi: 10.1080/10473289.2006.10464485

Pope, C. A. III, Turner, M. C., Burnett, R. T., Jerrett, M., Gapstur, S. M., Diver, W. R., et al. (2015). Relationships between fine particulate air pollution, cardiometabolic disorders, and cardiovascular mortality. *Circ. Res.* 116, 108–115. doi: 10.1161/CIRCRESAHA.116.305060

Postma, D. S., and Rabe, K. F. (2015). The asthma–COPD overlap syndrome. *N. Engl. J. Med.* 373, 1241–1249. doi: 10.1056/NEJMra1411863

Rawlins, B. G., McGrath, S. P., Scheib, A. J., Breward, N., Cave, M., Lister, T. R., et al. (2012). *The Advanced Soil Geochemical Atlas of England and Wales*. Keyworth: British Geological Survey.

Robertson, D. J., Taylor, K. G., and Hoon, S. R. (2003). Geochemical and mineral magnetic characterisation of urban sediment particulates, Manchester, UK. *Appl. Geochem.* 18, 269–282. doi: 10.1016/S0883-2927(02)00125-7

Robinson, S. G. (1986). The late Pleistocene palaeoclimatic record of North Atlantic deep-sea sediments revealed by mineral-magnetic measurements. *Phys. Earth Planet. Int.* 42, 22–47. doi: 10.1016/S0031-9201(86)80006-1

Rockström, J., Steffen, W., Noone, K., Persson, Å., Chapin, F. S., Lambin, E. F., et al. (2009). A safe operating space for humanity. *Nature* 461, 472–475. doi: 10.1038/461472a

Rohde, R. A., and Muller, R. A. (2015). Air pollution in China: mapping of concentrations and sources. *PLoS One* 10:e135749. doi: 10.1371/journal.pone.0135749

Roney, N., Osier, M., Paikoff, S. J., Smith, C. V., Williams, M., and De Rosa, C. T. (2016). ATSDR evaluation of the health effects of zinc and relevance to public health. *Toxicol. Ind. Health* 22, 423–493. doi: 10.1177/0748233706074173

Rose, N. L. (1994). A note on further refinements to a procedure for the extraction of carbonaceous fly-ash particles from sediments. *J. Paleolimnol.* 11, 201–204. doi: 10.1007/BF00686866

Rose, N. L. (2008). Quality control in the analysis of lake sediments for spheroidal carbonaceous particles. *Limnol. Oceanogr. Methods* 6, 172–179. doi: 10.4319/lom.2008.6.172

Rose, N. L. (2015). Spheroidal carbonaceous fly ash particles provide a globally synchronous stratigraphic marker for the Anthropocene. *Environ. Sci. Technol.* 49, 4155–4162. doi: 10.1021/acs.est.5b00543

Rose, N. L., and Appleby, P. G. (2005). Regional applications of lake sediment dating by spheroidal carbonaceous particle analysis I: United Kingdom. *J. Paleolimnol.* 34, 349–361. doi: 10.1007/s10933-005-4925-4

Rose, N. L., Juggins, S., and Watt, J. (1999). The characterisation of carbonaceous fly-ash particles from major European fossil-fuel types and applications to environmental samples. *Atmos. Environ.* 33, 2699–2713. doi: 10.1016/S1352-2310(98)00312-4

Rose, N. L., Rose, C. L., Boyle, J. F., and Appleby, P. G. (2004). Lake-sediment evidence for local and remote sources of atmospherically deposited pollutants on Svalbard. *J. Paleolimnol.* 31, 499–513. doi: 10.1023/B:JOPL.0000022548.97476.39

Shi, J., Huang, W., Chen, P., Tang, S., and Chen, X. (2018). Concentration and distribution of cadmium in coals of China. *Minerals* 8:48. doi: 10.3390/min8020048

Silva, R. A., West, J. J., Zhang, Y., Anenberg, S. C., Lamarque, J.-F., Shindell, D. T., et al. (2013). Global premature mortality due to anthropogenic outdoor air pollution and the contribution of past climate change. *Environ. Res. Lett.* 8, 34005–34012. doi: 10.1088/1748-9326/8/3/034005

Singh, K. P., Malik, A., Sinha, S., Singh, V. K., and Murthy, R. C. (2005). Estimation of source of heavy metal contamination in sediments of Gomti River (India) using principal component analysis. *Water Air Soil Pollut.* 166, 321–341. doi: 10.1007/s11270-005-5268-5

Speak, A. F., Rothwell, J. J., Lindley, S. J., and Smith, C. L. (2012). Urban particulate pollution reduction by four species of green roof vegetation in a UK city. *Atmos. Environ.* 61, 283–293. doi: 10.1016/j.atmosenv.2012.07.043

Swindles, G. T., Watson, E., Turner, T. E., Galloway, J. M., Hadlari, T., Wheeler, J., et al. (2015). Spheroidal carbonaceous particles are a defining stratigraphic marker for the Anthropocene. *Sci. Rep.* 5:10264. doi: 10.1038/srep10264

Taubes, G. (1995). Epidemiology faces its limits. *Science* 269, 164–169. doi: 10.1126/science.7618077

Teng, Y., Wu, J., Lu, S., Wang, Y., Jiao, X., and Song, L. (2014) Soil and soil environmental quality monitoring in China: a review. *Environ. Int.* 69, 177–199. doi: 10.1016/j.envint.2014.04.014

Thevenon, F., Graham, N. D., Chiaradia, M., Arpagaus, P., Wildi, W., and Poteì, J. (2011). Local to regional scale industrial heavy metal pollution record in sediments of large freshwater lakes in central Europe (Lakes Genva and Lucerne) over the last centuries. *Sci. Total Environ.* 412–413, 239–247. doi: 10.1016/j.scitotenv.2011.09.025

Thompson, R. (1980). Environmental applications of magnetic measurements. *Science* 207, 481–486. doi: 10.1126/science.207.4430.481

Tong, L. (1995). Element abundances of China's continental crust and its sedimentary layer and upper continental crust. *Chinese J. Geochem.* 14, 26–32. doi: 10.1007/BF02840380

Vaněk, A., Grösslová, Z., Mihaljevič, M., Trubač, J., Ettler, V., Teper, L., et al. (2016). Isotopic tracing of thallium contamination in soils affected by emissions from coal-fired power plants. *Environ. Sci. Technol.* 50, 9864–9871. doi: 10.1021/acs.est.6b01751

Venners, S. A., Wang, B., Xu, Z., Schlatter, Y., Wang, L., and Xu, X. (2003). Particulate matter, sulfur dioxide, and daily mortality in Chongqing, China. *Environ. Health Perspect.* 111, 562–567. doi: 10.1289/ehp.5664

Vesely, J., Almquist-Jacobson, A., Miller, L. M., Norton, S. A., Appleby, P., Dixit, A. S., et al. (1993). The history and impact of air pollution at Čertovo Lake, southwestern Czech Republic. *J. Paleolimnol.* 8, 211–231. doi: 10.1007/BF00177857

Walden, J., Oldfield, F., and Smith, J. (1999). *Environmental Magnetism: A Practical Guide. Technical Guide, No.* 6. London: Quaternary Research Association.

Wang, J., Li, S., Li, H., Qian, X., Li, X., Liu, X., et al. (2017). Trace metals and magnetic particles in PM2.5: magnetic identification and its implications. *Sci. Rep.* 7:9865. doi: 10.1038/s41598-017-08628-0

Wong, I. C., Ng, Y. K., and Lui, V. W. (2014). Cancers of the lung, head and neck on the rise: perspectives on the genotoxicity of air pollution. *Chinese J. Cancer* 33, 476–480. doi: 10.5732/cjc.014.10093

World Health Organisation (2014a). *7 Million Premature Deaths Annually Linked to Air Pollution.* Available at: http://www.who.int/mediacentre/news/releases/2014/air-pollution/en/ [accessed January 29, 2018].

World Health Organisation (2014b). *Ambient (outdoor) Air Pollution in Cities Database 2014.* Available at: http://www.who.int/phe/health_topics/outdoorair/databases/cities/en/ [accessed March 28, 2018].

Wu, Y. (2005). Dating recent lake sediments using spheroidal carbonaceous particle (SCP). *Chinese Sci. Bull.* 50, 1016–1015. doi: 10.1360/982004-321

Xiaoyan, S., Longyi, S., Shushen, Y., Riying, S., Limei, S., and Shihong, C. (2015). Trace elements pollution and toxicity of airborne PM10 in a coal industrial city. *Atmos. Pollut. Res.* 6, 469–475. doi: 10.5094/APR.2015.052

Yang, T., Liu, Q., Li, H., Zeng, Q., and Chan, L. (2010). Anthropogenic magnetic particles and heavy metals in road dust: magnetic identification and its implications. *Atmos. Environ.* 44, 1175–1185. doi: 10.1016/j.atmosenv.2009.12.028

Yang, T., Liu, Q., Zeng, Q., and Chan, L. (2009). Environmental magnetic responses of urbanization processes: evidence from lake sediments in East Lake, Wuhan, China. *Geophys. J. Int.* 179, 873–886. doi: 10.1111/j.1365-246X.2009.04315.x

Yao, S., and Xue, B. (2013). Heavy metal records in the sediments of Nanyihu Lake. China: influencing factors and source identification. *J. Paleolimnol.* 51, 15–27. doi: 10.1007/s10933-013-9752-4

Yongguan, C., Seip, H. M., and Vennemo, H. (2001). The environmental cost of water pollution in Chongqing, China. *Environ. Dev. Econ.* 6, 1–21. doi: 10.1017/S1355770X01000183

Yunginger, R., Bijaksana, S., Dahrin, D., Zulaikah, S., Hafidz, A., Kirana, K., et al. (2018). Lithogenic and anthropogenic components in surface sediments from Lake Limboto as shown by magnetic mineral characteristics, trace metals, and REE Geochemistry. *Geosciences* 8:116. doi: 10.3390/geosciences8040116

Zeng, L., Ning, D., Xu, L., Mao, X., and Chen, X. (2015). Sedimentary evidence of environmental degradation in Sanliqi Lake, Daye City (a typical mining city, central China). *Bull. Environ. Contam. Toxicol.* 95, 317–324. doi: 10.1007/s00128-015-1606-5

Zhang, M., Song, Y., Cai, X., and Zhou, J. (2008). Economic assessment of the health effects related of particulate matter pollution in 111 Chinese cities by using economic burden of disease analysis. *J. Environ. Manage.* 88, 947–965. doi: 10.1016/j.jenvman.2007.04.019

Zhang, W., Ming, Q., Shi, Z., Chen, G., Niu, J., Lei, G., et al. (2014). Lake sediment records on climate change and human activities in the Xingyun Lake Catchment, SW China. *PLoS One* 9:e102167. doi: 10.1371/journal.pone.0102167

Zhao, P., Dai, M., Chen, W., and Li, N. (2010). Cancer trends in China. *Jpn. J. Clin. Oncol.* 40, 281–285. doi: 10.1093/jjco/hyp187

Conflict of Interest Statement: The authors declare that the research was conducted in the absence of any commercial or financial relationships that could be construed as a potential conflict of interest.